



**ROYAL INSTITUTE
OF TECHNOLOGY**

Tunable Phase-shifted fiber Bragg gratings and its applications in the microwave region

Patrik Rugeland



Master of Science Thesis

Department of Applied Physics
School of Engineering Sciences
Royal Institute of Technology

Stockholm, Sweden 2009

TRITA-FYS: 2009:26
ISSN: 0280-316X
ISRN: KTH/FYS/-09:26-SE

Abstract

A phase-shifted fiber Bragg grating is an in-fiber optical filter that transmits a very narrow linewidth within a much broader reflection spectrum. By manufacturing the grating in a fiber with internal electrodes it is possible to vary the transmitted wavelength by applying electrical voltage to the electrodes, and then achieve tunable filtering.

In this thesis, the FBG component is used in two closely related applications; microwave frequency measurement and photonic microwave generation.

The frequency measurement is done by converting a microwave signal of unknown frequency to the optical domain through optical modulation of an optical carrier. The spectrum of the optical signal will then consist of three peaks where the wavelength of the central peak is known beforehand. The wavelength distance between the central peak and the side-peaks arising from the modulation is directly proportional to the modulation frequency. Thus by measuring the wavelength of one of the side-peaks, the modulation frequency is readily at hand. This is done by sweeping the narrow linewidth FBG filter through the possible wavelengths by applying a short high voltage pulse to the internal electrodes and measuring when a signal is transmitted through the filter. Experiments showed that the component successfully measured frequencies between 2.5-8.5 GHz.

The second application is a novel configuration for photonic microwave generation, where the birefringence of the component is used to create a polarization-split ring-laser cavity which operates at dual wavelengths. The microwave frequency is generated by beating the two wavelengths at a detector. The experiments showed that the setup could generate a beat frequency at ~5.5 GHz for a long period of time. By varying the birefringence of the component with the help of the internal electrodes it was also possible to controllably vary the beat frequency ~100 MHz.

Sammanfattning

Ett fasskiftat fiber Bragg gitter är ett intra-fiber optiskt filter vars reflektionsspektra är ett brett stoppband med en väldigt smal transmissionstopp i mitten. Om gittret är tillverkat i en fiber med elektroder är det möjligt att variera våglängden för reflektionsspektrumet genom att koppla en elektrisk spänning till elektroderna. Detta möjliggör avstämbar optisk filtrering.

I denna rapport används fiber Bragg gittret inom två snarlika tillämpningar; frekvensmätning av mikrovågor samt optisk generering av mikrovågor.

Frekvensmätningen genomförs genom att omvandla en mikrovågssignal med okänd frekvens till den optiska domänen med hjälp av intensitetsmodulering av en optisk bärare. Våglängdsspektrumet för den optiska signalen kommer då att bestå av tre toppar där mittentoppen har en känd våglängd. Våglängdsskillnaden mellan mittentoppen och sidotopparna, som uppstår på grund av modulationen, är direkt proportionellt mot modulationsfrekvensen. Detta gör att man kan bestämma modulationsfrekvensen genom att endast mäta våglängden för endera sidotoppen. Denna mätning görs genom att svepa det smalbandiga FBG filtret genom de möjliga våglängder där sidotoppen kan finnas, genom att lägga på en kort högspänningspuls på fiberelektroderna och mäta vid vilken tid som en signal släpps igenom filtret. Det visade sig i experiment att komponenten kunde användas för att mäta frekvenser mellan 2,5-8,5 GHz.

Den andra tillämpningen av FBG komponenten är en nydanande uppställning för optisk generering av mikrovågor. Komponentens dubbelbrytning används för att bygga en polarisationsdelad ringlaser kavitet som lasrar vid dubbla våglängder. Mikrovågsfrekvensen generas genom att superponera båda våglängderna på en detektor så att skillnadsfrekvensen erhålls. Det visade sig i experiment att uppställningen kunde generera en stabil mikrovågssignal med frekvens $\sim 5,5$ GHz under en relativt lång tid. Genom att ändra på komponentens dubbelbrytning med hjälp av fiberelektroderna, var det möjligt att kontrollerbart variera mikrovågsfrekvensen ~ 100 MHz.

Acknowledgement

First I would like to thank my supervisor Walter Margulis at Acreo, who has been a great source of inspiration and support throughout this diploma work. He has given me hands-on assistance in the lab environment as well as invaluable feedback to my thesis.

Many thanks to Kurt Westermark and Göran Tengstrand, my supervisors at Saab Avitronics, for the opportunity to conduct this diploma work. They both gave me valuable insights into the field of radar and microwave applications.

I am thankful to Göran Manneberg, my supervisor at KTH, who showed great confidence in my work.

I would specially like to thank Carola Sterner, who helped me manufacture the fiber Bragg gratings in the metal-filled fiber needed in my experiments and Oleksandr Tarasenko who performed the delicate work of mounting and contacting the metal-filled fiber.

I am grateful towards Zhangwei Yu for her input towards the procedures of my experiments as well as allowing me to borrow some of her unique optical components for my measurements.

I would also like to thank Mikael Malmström for generously sharing his workspace and lab equipment with me.

Finally I would like to thank all my colleagues at Acreo AB for the pleasant and rewarding work environment that I had a chance to experience during my diploma work.

Patrik Rugeland
Stockholm, June 2009

Contents

Abstract	i
Sammanfattning	ii
Contents.....	v
1. Introduction	1
1.1. Background	1
1.2. Purpose and goal	1
1.3. Summary and disposition	2
2. Radar parameters.....	3
2.1. Basic Radar Principle	3
2.2. Carrier frequency and bandwidth.....	3
2.3. Pulse width and pulse repetition frequency.....	3
3. Some common optical components and equipment.....	5
3.1. Optical fiber, general overview	5
3.2. Special fiber design	6
3.3. Metal-filled fibers.....	7
3.4. Fiber-optical couplers.....	9
3.5. Isolator.....	10
3.6. Circulator.....	11
3.7. Polarization controller (PC)	11
3.8. Fabry-Perot etalon	12
3.9. Electrical Spectrum Analyzer (ESA)	12
3.10. Optical Spectrum Analyzer (OSA)	13
3.11. Photodetector.....	13
3.12. Tunable light source (TLS)	14
3.13. Erbium-doped Fiber Amplifier (EDFA)	14
3.14. Optical Modulator	15
3.15. Calculations of Mach-Zehnder Modulator.....	16
4. Fiber Bragg grating (FBG).....	17
4.1. Properties of fiber Bragg gratings	17
4.2. Variations of fiber Bragg gratings.....	18
4.2.1. Chirped grating.....	18
4.2.2. Apodized grating.....	18
4.2.3. Phase-shifted FBG.....	20
4.2.4. Birefringent FBG.....	20
4.3. Optimizing desired FBG for tunable GHz filter.....	21
5. Tuning fiber Bragg grating.....	23
5.1. Altering the pitch of the FBG.....	23
5.2. Altering the refractive index of the FBG	24
5.3. Tuning of metal filled fiber Bragg grating.....	24
6. Rapid optical scan of the microwave spectrum.....	27
6.1. Suppression of optical carrier.....	27
6.1.1. Double pass through transmitting fiber Bragg grating.....	27
6.1.2. Additional suppression of the optical carrier using two very similar FBGs	29
6.1.3. Single sideband filtering using ultra-narrow phase-shifted FBG.....	30
6.2. Setup for determining the RF-frequency of a modulated optical signal	31
6.3. Thermal stability of system	32
6.4. Results	33
6.5. Conclusion.....	34

7.	Microwave generation using tunable phase-shifted FBG	35
7.1.	Setup for polarization-split cavity for dual wavelength operation.....	35
7.2.	Time-varying optical microwave generation	37
7.3.	Results	38
7.3.1.	Static measurements	38
7.3.2.	Time-varying measurements	39
7.4.	Conclusion.....	39
8.	General Conclusion and Future Work.....	41
	References	43

1. Introduction

There has been a large interest in utilizing optical carriers to study microwave signals. [1,2,3]. A great deal of effort has been made in order to properly modulate the optical carrier with the microwave frequency [4,5,6]. Studies have also been done to measure microwave frequencies with optical components through an amplitude comparison function [7,8,9]. There has also been progress in using optical signals to generate microwave signals by beating two optical signals [10,11,12,13,14,15]. In this work, two different applications of a tunable fiber Bragg grating, related to optical microwave signals are demonstrated.

The first application uses a phase-shifted fiber Bragg grating as a tunable filter in order to measure the microwave frequency of a modulated optical carrier. The microwave frequency in question is a received radar signal that is to be analyzed. The second application uses a tunable birefringent phase-shifted fiber Bragg grating in order to operate an Er^{3+} fiber ring laser at two wavelengths simultaneously, which are mixed to generate a tunable microwave signal.

1.1. Background

The use of microwave technologies has been developed throughout the last century, both in the field of communication over radio as well as detection with radar. However, the improvements in the field of photonics have provided several opportunities that have been examined for the past decades. For instance, the low-loss transmission and large bandwidth of optical fibers provides long-distance communication with large information density at low cost. The cross-disciplinary field of microwave photonics which has been developed alongside the field of photonics examines the use of photonics for microwave applications. It deals both with the possibility to convert a microwave signal to the optical domain as well as directly generating microwave signals from optical signals. One of the key photonic components is the fiber Bragg grating which provides an accurate wavelength filtering and can be used for very sensitive environmental measurements.

The development of radar warning systems has been carried out alongside the development of radar systems. The main purpose of radar warning systems is to detect the characteristics and location of the radar source in order to assess and counteract threats to the platform. As radar systems have become more sophisticated, given more advanced digital processing of the radar signal as well as incorporated improved radar transmitters and receivers, the need for faster and more accurate radar warning systems increased.

1.2. Purpose and goal

The purpose of this thesis was to examine the possibility to utilize the features of the optical domain in order to detect and determine the frequency of radar signals with sufficient accuracy and selectivity. One striking feature of the optical domain is the low loss in optical fibers. A coaxial cable can have attenuation of the order of $\sim 0.1\text{-}1$ dB/m, while a standard optical fiber only has a loss of ~ 0.2 dB/km. This feature makes it possible to produce a replica of a signal and delay it by propagation in a long fiber length where the delayed signal suffers low attenuation. It then becomes possible to conduct two consecutive measurements on the same signal with a delay between them. The first measurement can be used to acquire some a priori knowledge of the signal in order to perform a more accurate measurement on the delayed signal. If the delay line is 20 km, the delay of the signal will be 100 μs with only a loss of 4 dB.

Another significant difference between the RF and the optical domain is the frequencies associated with the signal. An optical signal, with a wavelength of $\lambda \sim 1.5$ μm , has a frequency of $\nu \sim 2 \times 10^{14}$ Hz (2×10^5 GHz). The frequency range of the microwave signal is only $\nu \sim 2\text{-}$

20 GHz, i.e. roughly 10^4 - 10^5 times smaller than the optical frequencies. Thus a very small shift in the optical domain will yield great changes in the microwave domain.

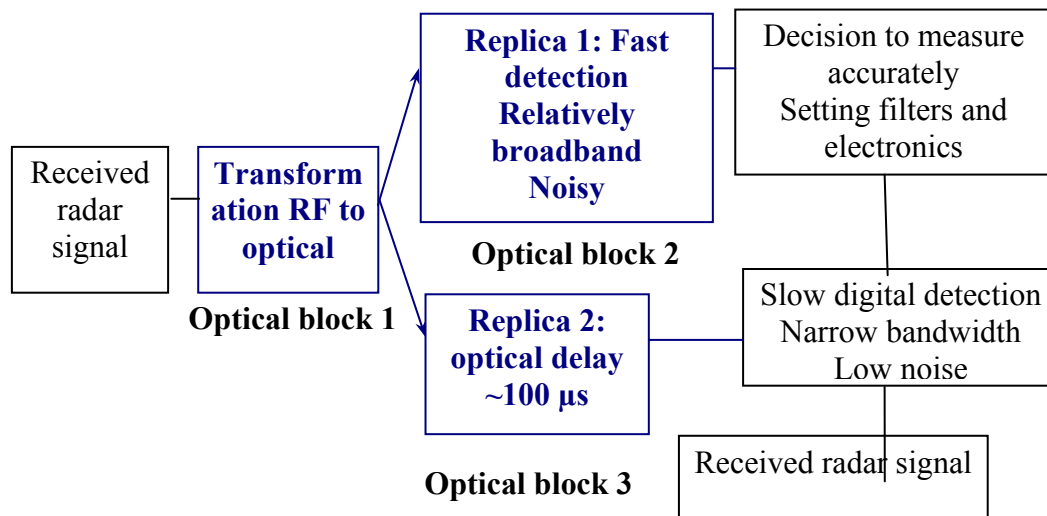


Figure 1. Block diagram of photonic detection of radar signal

The block diagram in Figure 1 depicts the intended setup. The incoming radar signal is obtained with a very wideband and wide-lobe antenna and is transformed into an electrical signal. This signal is fed into an intensity modulator that transforms the signal from the RF-domain into the optical domain in Optical block 1. After the transformation, the signal is divided into two separate parts where replica 1 is subjected to a rapid detection in Optical block 2, to determine an approximate frequency of the RF-signal. Replica 2 is delayed in a long optical fiber in Optical block 3 and then detected with a more accurate digital filter. The frequency information from the measurement in Optical block 2 is used to adjust the detectors of Replica 2 to the correct frequency range.

This thesis is mainly focused on the realization of the rapid optical detection of the RF-signal in Optical Block 2. However, during the development of the optical components, an alternative application of the component was considered, where microwave signals were generated directly from the optical domain.

1.3. Summary and disposition

As this thesis is an experimental study of a novel measurement technique, the main focus was placed on the experiments. This is reflected in the report, where the fundamental theory and the derivation of the governing equations is very abbreviated.

Chapter 2 briefly describes the basic principles of radar systems and the key parameter associated with the systems.

Chapter 3 describes the various optical components used in the experiments. The level of details varies depending on the significance of the component.

Chapter 4 and 5 describes the principle and the application of the fiber Bragg grating respectively. As the fiber Bragg grating is the most central component for this thesis, additional notice has been taken to its characteristics.

Chapter 6 describes the microwave measurement using the special fiber Bragg grating, where the filter successfully detected signals in the frequency range 2.5-8.5 GHz within less than 2 milliseconds.

Chapter 7 describes a tunable microwave generation from an optical source using a novel configuration with a special FBG along with standard optical amplifiers. The system manages ~ 200 MHz tuning with stable microwave generation at ~ 5 GHz.

2. Radar parameters

Radar warning systems are designed to quickly detect and characterize hostile radar signals to determine the type of radar as well as its position. This in order to discern what threat it poses to be able to engage countermeasures or evasive action. The current technology utilizes microwave receivers and signal processing to determine the amplitude, frequency and pulse-length of the signal as well as direction and distance to the transmitter. In general, the radar pulse is composed of a few simple waveforms but can vary significantly between different applications and even between different pulses. However there are a few characteristic parameters that must be fulfilled in order for the radar to operate properly.

2.1. Basic Radar Principle

Radar is an acronym for *radio detection and ranging*. A radar consists of an antenna that transmits microwave pulses and receives the reflections from various objects. By analyzing the returning signal, it is possible to discern certain characteristics of the reflecting objects. This chapter will present a brief description of the basic principles of radars. However, several of the more complicated features are omitted since they are out of the scope for this thesis.

2.2. Carrier frequency and bandwidth

The purpose of a radar is to detect and locate objects using reflected radio signals. The time, t , it takes for a signal to travel a distance R from the antenna, to the target and back to the antenna again is determined by:

$$t = \frac{2R}{c} \quad (1)$$

where c is the speed of light. Thus the distance to the object is directly related to the time it takes before the reflected signal is detected. However, in order to detect relatively small objects, the resolution in distance needs to be sufficient:

$$\Delta t = \frac{2\Delta R}{c} \quad (2)$$

which directly corresponds to resolution in time. If the resolution in distance is to be $\Delta R=15$ m, the required resolution in time must be $\Delta t=0.1$ μ s. As the instantaneous pulse bandwidth is inversely proportional to the resolution in time; $B = 1/\Delta t$ the corresponding bandwidth will be $B=10$ MHz.

The carrier frequency of the radar signal is normally $\nu = 2-18$ GHz. This corresponds to a wavelength of $\lambda \sim 1.6-15$ cm which is much smaller than any of the requirements for distance resolution. Thus the precise frequency of the radar signal is not determined by the requirements for the performance of the radar. Different radar systems can operate at different carrier frequencies and some radar systems can even change its carrier frequency between different pulses. Thus in order to ensure that all signals are detected, the entire spectrum of $\nu = 2-18$ GHz needs to be covered with the resolution of $B\sim 10$ MHz at every pulse.

2.3. Pulse width and pulse repetition frequency

A standard radar normally uses the same antenna for transmission and receiving. As the reflected signal is several orders of magnitude weaker than the transmitted signal, it is usually not possible to receive while transmitting. Thus, the radar transmits a short radar pulse with very high pulse power. A typical pulse width could be $T=0.1$ μ s which would directly correspond the desired distance resolution of $\Delta R=15$ m. However, it is often not possible or

desirable to achieve sufficient pulse energy without extremely high pulse power. Instead, it is possible to use several consecutive pulses, separated in frequency or phase, in a process known as pulse compression to distribute the energy over a longer period of time, while maintaining the bandwidth. This process is commonly used but is out of scope for this thesis. The typical radar pulse width is $T=0.2-20 \mu\text{s}$. However, another aspect regarding the radar pulse width is the interesting range. If the pulse is very long, it is not possible to detect signals that return during the transmission of the subsequent pulse. For a $T = 20 \mu\text{s}$ pulse, the minimum distance that can be detected will be:

$$R = \frac{cT}{2} = \frac{3 \times 10^8 \times 2 \times 10^{-5}}{2} = 3\text{km} \quad (3)$$

As for shorter distances, the pulse energy does not need to be as large since the solid angle of the target is much larger. The solid angle of a radar target will scale as $1/R^2$ of the distance from the antenna to the target. Likewise, the solid angle of the receiver from the radar target will also scale as $1/R^2$. Thus the reflected power from the radar targets that reach the receiver will scale as $1/R^4$ with the distance between the antenna and the target.

The pulse repetition frequency (PRF) f_R determines how many pulses are transmitted per second and is inversely proportional to the pulse repetition interval (PRI) T_R .

$$f_R = \frac{1}{T_R} \quad (4)$$

As this is a limit to how long the antenna shall receive before the next pulse is transmitted, the PRI provides the largest unambiguous distance that can be detected.

$$R_1 = \frac{cT_R}{2} = \frac{c}{2f_R} \quad (5)$$

For $f_R = 1 \text{ kHz}$, $T_R = 1 \text{ ms}$, the maximum unambiguous distance is $R_1 = 150 \text{ km}$. For $f_R = 100 \text{ kHz}$, $T_R = 10 \mu\text{s}$ the distance is $R_1 = 1.5 \text{ km}$.

The duty cycle $\eta=T/T_R$, determines the proportion between the pulse length and the pulse repetition interval. Normally, the duty cycle varies between $\eta = 0.1-10 \%$ for different types of radar systems. However, it is possible to use a radar system that transmits a continuous wave, where the transmitted and receiver operates simultaneously. This is either done by sufficiently isolate the transmitted signal from the received signal or by using different antennas for transmitting and receiving.

3. Some common optical components and equipment

There are great many different optical components and only a few of them are described in this chapter. The fiber optic components that guide, direct or filter the light in some manner are described briefly. A few different detectors are then described along with the different light sources used. The optical modulator used is described in a bit more detail as this component is crucial to the experiment. All of these components as commercially available, except the metal filled fibers which are made in-house at Acreo.

3.1. Optical fiber, general overview

An optical fiber is an optical waveguide based on the principle of *total internal reflection*. In general, a proper description of the characteristics of an optical fiber is derived by solving the Maxwell’s equations. However, in order to get a general overview of the function of an optical fiber, it is suffice to consider the approximations of geometrical optics.

In geometrical optics, Snell’s law dictates that light passing through an interface between two different materials refracts according to the relation:

$$n_1 \sin \theta_i = n_2 \sin \theta_t \tag{6}$$

where n_1 and n_2 are the refractive indices of the two materials and θ_i and θ_t are the incidence and transmission angle respectively. If $n_1 > n_2$, then $\theta_t > \theta_i$, that is, if the first material have a higher refractive index than the second material, the transmission angle will be larger than the incidence angle. If the incidence angle is as large that the transmission angle would be $\theta_t \geq 90^\circ C$, no light can be transmitted and instead all light will be reflected. This angle is called the critical angle.

$$\sin \theta_c = \frac{n_2}{n_1} \tag{7}$$

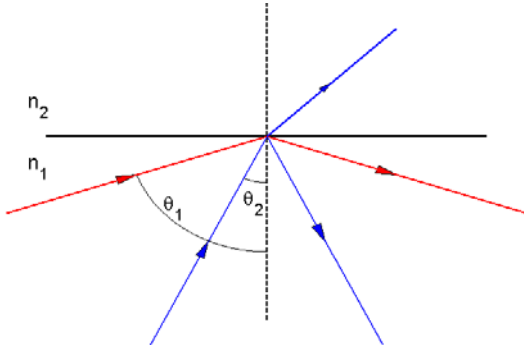


Figure 2. Refraction and reflection at interface between material above (red) and below (blue) the critical angle

An optical fiber consists of a wave-guiding core, surrounded by a cladding. The core has a slightly higher index of refraction than the cladding which confines the light to the core through total internal reflection.

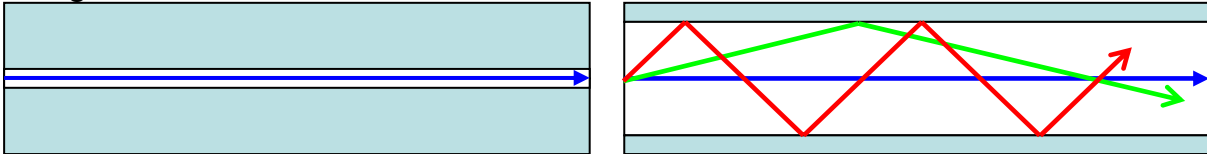


Figure 3. Propagation in a (a) Single-mode fiber, (b) Multi-mode fiber

In general, the notion of total internal reflection and the use of geometrical optic are only valid while the optical wavelength is small compared to all relevant distances. In a standard telecom fiber, the core diameter is $\sim 10 \mu\text{m}$, which is comparable to the optical wavelength $\lambda \sim 1.5 \mu\text{m}$. By evaluating the Maxwell's equations it is possible to show that there is only a single transverse mode which can be guided by the core and these fibers are known as single mode fibers (SMF) as seen in Figure 3 (a). In Figure 3 (b) there are several paths that the light can propagate which corresponds to different transverse modes that can be guided by the fiber. This is known as a multi-mode fiber (MMF). As the index of refraction of the fiber is $n \sim 1.45$, the propagation speed of the light will be:

$$v = \frac{c}{n} \approx 2 \times 10^8 \text{ m/s} \tag{8}$$

As all of the light is confined to the core, as long as the fiber is not bent too much, the light can propagate a very long distance with very low loss, in the order of 0.2-1 dB/km.

A standard telecom optical fiber usually has a core diameter of $\sim 10 \mu\text{m}$ and a cladding with an external diameter of $\sim 125 \mu\text{m}$ and can be manufactured to be several kilometers long. However, these measurements can be widely varied when manufacturing the fiber to obtain desired properties. It is also possible to splice two optical fiber together using high-precision tools.

3.2. Special fiber design

An optical fiber is made from preform which is a thick glass rod with a diameter of a few centimeters and a length of approximately one meter. When manufacturing the fiber, the preform is placed vertically and heated to around 2000 °C, so that the glass softens making it possible to draw a thin fiber from the tip of the preform. By controlling the heat of the furnace and the speed of the drawing, it is possible to achieve the desired outer diameter with very high precision. The preform itself has the same proportions as the final optical fiber will have. If the diameter of the cladding is to be 10 times larger than the diameter of the core, the same proportions should exist in the preform. It is also possible to achieve much more complex structures in a fiber, simply by designing the preform accordingly. By drilling holes in the preform and pressurizing them while drawing the fiber it is possible to obtain a fiber with holes in it, as seen in Figure 4 [16]. Naturally, there are numerous other fiber configurations that are possible to achieve but they will not be covered in this thesis.

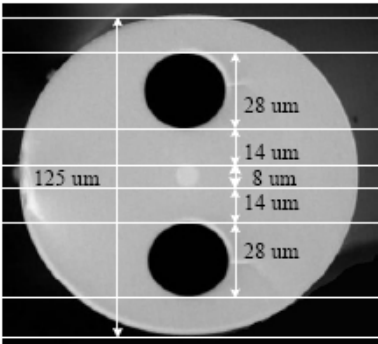


Figure 4. Cross-section of the twin-hole fiber used (SEM picture)

3.3. Metal-filled fibers

It is possible to manufacture optical fibers with electrodes inside the cladding by filling the holes of a fiber with a metal. This is done by melting the metal and forcing it into the holes with high pressure and then let it cool to a solid. The metal used for this thesis is an eutectic alloy; $\text{Bi}_{47}\text{Sn}_{53}$, with the melting point $137\text{ }^{\circ}\text{C}$. The principle of the metal-filling of the fiber holes is shown in Figure 5 [17].

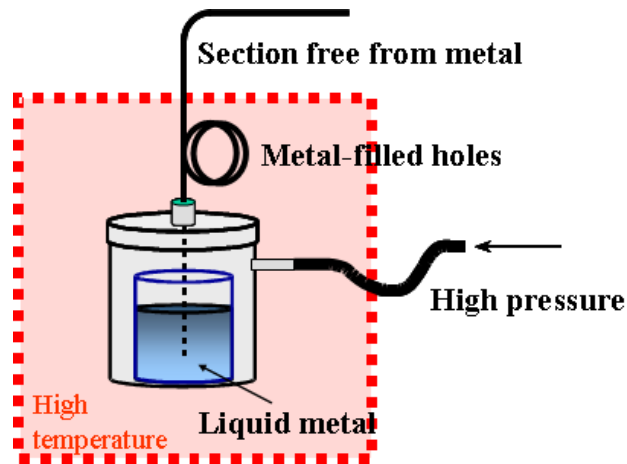


Figure 5. Method to fill holey fibers with metal

When the holes of the fiber have been filled with metal, it is possible to connect these metal columns with wires. This is done by side-polishing the fiber to expose the metal-filled holes.

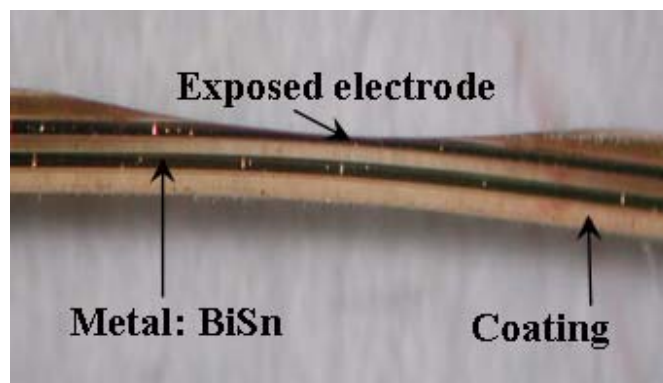


Figure 6. Picture of side-polished metal-filled fiber

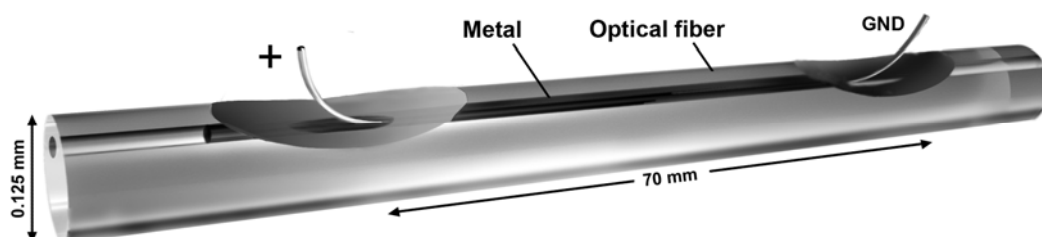


Figure 7. Schematic picture of metal-filled fiber with contacted wires.

As the internal electrodes of the fiber have been connected to external wires, it is possible to apply an electrical current through them. The resistance of the metal column is, for the component used in this thesis, $\sim 43\ \Omega$. Due to the resistive load, some energy will be

deposited in the electrode by the applied electricity which will heat the electrodes. If too much energy is deposited, the temperature of the electrodes can increase above the melting point ($\sim 137^\circ\text{C}$) and there is a risk that the metal column will break and form micro-fissures. If this happens, the connection will be broken and the electrical current can no longer pass through the electrode. As a rule of thumb based on empirical experience, the internal electrodes can sustain 100 mA, i.e. ~ 4 V DC without breaking. However, by applying a very short pulse with low repetition rate the voltage can be significantly increased. By considering the adiabatic process, where the pulse is assume too short for any heat to have time to dissipate during the pulse, an upper limit to the voltage of the pulse can be found.

The heat required to increase the temperature of the metal column ΔT is:

$$Q = Cm\Delta T = C\rho L\pi r^2 \Delta T \quad (9)$$

Whereas the heat deposited during a Δt long square pulse with voltage U is:

$$Q = \frac{U^2}{R} \Delta t \quad (10)$$

thus:

$$C\rho L\pi r^2 \Delta T = \frac{U^2}{R} \Delta t \quad (11)$$

where [23]:

Heat capacity [$\text{Jkg}^{-1}\text{K}^{-1}$]	$C = 167$
Density [kgm^{-3}]	$\rho = 8560$
Length of metal column [cm]	$L = 7$
Radius of metal column [μm]	$r = 14.4$
Electrical resistance of metal column [Ω]	$R = 43$

Thus the electrical voltage needed will be:

$$U^2 = \frac{RC\rho L\pi r^2 \Delta T}{\Delta t} \approx 0.0028 \frac{\Delta T}{\Delta t} [\text{V}^2] \quad (12)$$

The maximum temperature increase from room temperature is $\Delta T \sim 110$ K, thus:

$$U^2 \approx \frac{0.3}{\Delta t} [\text{V}^2] \quad (13)$$

For a high voltage electrical pulse of $U = 1$ kV, the pulse length can be $\Delta t = 300$ ns.

The maximum pulse voltage available in the experiments for this thesis was $U = 20$ V. Thus, the maximum pulse length should not exceed $750 \mu\text{s}$. However, for near-millisecond pulses, the process is no longer adiabatic and some of the deposited energy will have dissipated during the pulse. The pulses used in the experiment were $250\text{-}350 \mu\text{s}$ long with a voltage of 20 V.

The adiabatic temperature change this would render is:

$$\Delta T \approx \frac{U^2 \Delta t}{0.0028} \approx 36 - 50 \text{ K} \quad (14)$$

However, the actual temperature increase will be significantly lower due to the dissipation of the heat.

3.4. *Fiber-optical couplers*

One of the most common fiber-optic components is the coupler. In essence, this component simply transfers some or all light from one optical fiber to another, depending on the characteristics of the component. The full derivation of this process is far from trivial, but an intuitive description is readily at hand. A schematic image of an optical coupler can be seen in Figure 8.

If two waveguides, such as fiber optical cores, are sufficiently close to each-other, the electromagnetic field from one core will couple and be transferred to the other. Likewise, it will be transferred back to the original core again. Thus, the light will effectively bounce between the two cores and at any given position it will be in either cores or partially in both. As the component is manufactured at a given length, light entering into one fiber will have a predefined distribution between the two exiting fiber arms. For instance, a 3 dB coupler is contrived so that 50 % of the light will be in either fiber at the end of the component. However, the periodicity of the coupling between the cores is highly dependent on both wavelength and refractive index so that different wavelengths will be distributed differently between the cores at a given position. For instance the Wavelength Division Multiplexer (WDM) in Figure 9 is manufactured so that $\lambda = 1550$ nm will only exit through fiber 1 while $\lambda = 1300$ nm will only exit through fiber 2. This is useful if two different wavelengths are to be separated from each other. Naturally, the coupler can be made to yield any distribution between the two fibers for a given wavelength by simply adjusting the length of the coupler while making it. For instance the 5% tap, allows only 5% of the light to exit through one of the fibers while 95 % of the light exits through the other.

It is also possible to make a polarization selective coupler by using a birefringent coupler. Because of the birefringence, the two orthogonal polarization states will experience different refractive indices and will thus couple between the two cores with different periodicity. By adjusting the length of the coupler it is possible to achieve a polarization splitter where one polarization state exits through fiber 1 and the other state exits through fiber 2. However, the coupler can also be used in reversed so that two orthogonal polarization states can be joined in the same fiber.

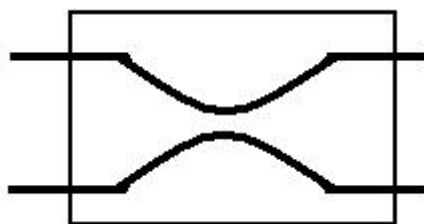
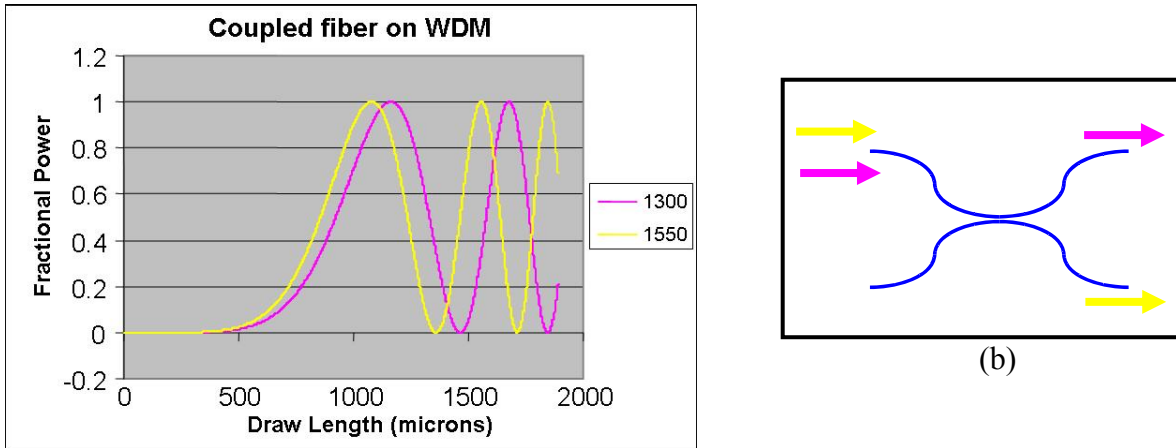


Figure 8. Schematic picture of a coupler with four ports. Input from either of the left ports will exit through both of the right ports. The power distribution between the output ports will depend on the configuration of the coupler.



(a)
Figure 9. (a) Fraction of light in fiber 2 as light enters fiber 1 at different positions for two different wavelengths, (b) Schematic picture WDM coupler

3.5. Isolator

An optical isolator is a component that only allows light to travel in one direction. The most common optical isolator is based on the Faraday rotator along with absorbing polarizers.

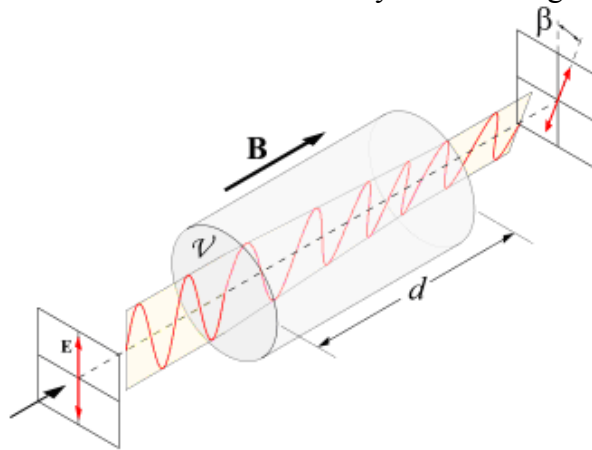


Figure 10. Faraday rotator with a polarizer and an analyzer (image from wikipedia.com)

For forward travelling light the polarizer only transmits vertically polarized light which is then rotated 45 degrees by the Faraday rotator. The analyzer is set to 45 degrees and will thus transmit all the forward travelling light. For backward travelling light, the analyzer only transmits the light polarized along the 45 degree axis and the Faraday rotator rotates the light an additional 45 degrees so that it is parallel to the horizontal axis. Thus it is absorbed by the polarizer and is prevented from propagating further.

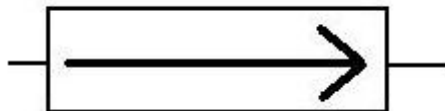


Figure 11. Schematic image of optical isolator. Light can only pass through the component in one direction, from left to right.

3.6. Circulator

A circulator is an optical component that is not reversible. The component has 3 ports and only allows light to travel in one direction; from port 1 to port 2 and from port 2 to port 3. Thus if light is entered through port 1, it will exit through port 2. If the light is reflected after port 2, it will be reenter the circulator and exit through port 3. The circulator is also based on Faraday rotator and polarizers, and can be purchased in polarization independent configurations.

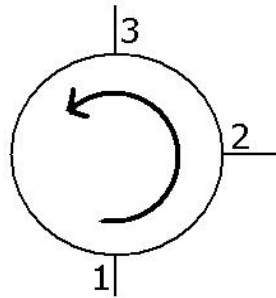


Figure 12. Schematic image of optical circulator. Light entering through port 1 will exit through port 2, light entering through port 2 will exit through port 3 and light entering through port 3 will be blocked.

3.7. Polarization controller (PC)

The fiber polarization controller is a component which rotates the polarization of the light in the fiber. As the light traverses through the optical fiber, any twist of the fiber induces a slight birefringence which can alter the polarization state. The polarization controller utilizes this effect in order to control the specific polarization state. The polarization controller has three loops on which the optical fiber is wired. Under proper condition of tension, if the fiber is wired one lap around a loop or correct diameter, it will induce a phase retardation of $\lambda/4$. In the polarization controller, the first and the last loop is wired with a single lap, while the middle loop is wired with two laps.

The setup of a $\lambda/4$ - $\lambda/2$ - $\lambda/4$ can in principle rotate the polarization to any other polarization state, regardless of the initial state. However, since the initial state is seldom precisely known, it is a matter of trial and error to obtain the desired polarization rotation.

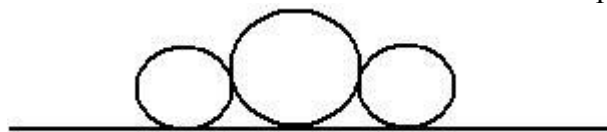


Figure 13. Schematic image of fiber-optic polarization controller

3.8. Fabry-Perot etalon

A Fabry-Perot etalon is a tunable optical filter consisting of two parallel, highly reflecting mirrors.

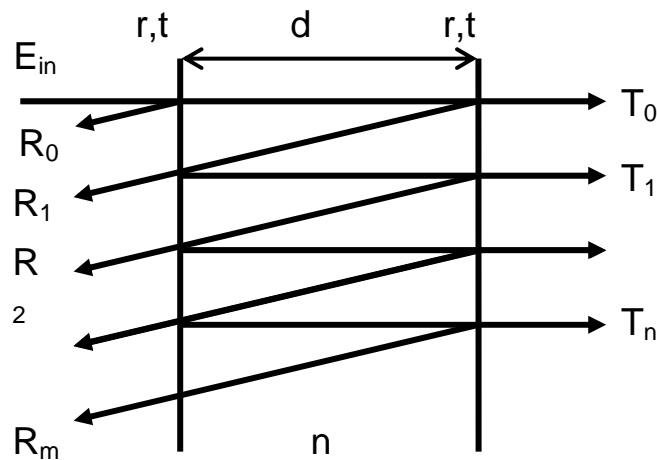


Figure 14. Schematic setup of Fabry-Perot etalon

As the light enters the filter, it will be reflected between the mirrors many times and only a very small fraction will leak out at every reflection. For one specific wavelength; $\lambda = 2nd$, the distance between the mirrors will be so that all the transmitted light T_i will be in phase. Likewise, all the light that leaks out in the back-direction R_{1-N} , will be out of phase with the initial reflection R_0 . Due to constructive and destructive interference, all the light will be transmitted through the filter for this wavelength. Neighboring wavelengths are blocked, and the Fabry-Perot etalon provides for spectral filtering. However, for shorter wavelengths that fulfill the condition $m\lambda = 2nd$, where m is an integer, will also be transmitted. Thus, if the distance d is much larger than wavelength, there are many closely adjacent wavelengths that are transmitted. All other wavelengths that are not in phase will simply be reflected with a small fraction that leaks through the filter. The bandwidth of the filter depends on both reflectance of the mirrors and the distance between them. However, the bandwidth of the filter is proportional to the separation between transmission peaks and thus a very narrow filter will have very many adjacent transmission peaks.

It is also possible to achieve a tunable Fabry-Perot etalon by allowing an adjustable optical path difference between the mirrors. This is most easily achieved by tilting the mirrors by an adjustable angle so that the transmitted wavelength will depend on the incidence angle of the light.

A typical Fabry-Perot filter is widely tunable and has a single 1-3 nm wide transmission band in the C-band. The component is often “pigtailed”, i.e. provided with input and output fiber connectors.

3.9. Electrical Spectrum Analyzer (ESA)

The electrical spectrum analyzer is a device that determines the frequency composition of an electrical signal. This is either achieved by a sweeping digital filter or through digital signal processing using fast Fourier transform (FFT). The resultant spectrum is the intensity distribution over frequencies.

3.10. Optical Spectrum Analyzer (OSA)

The optical spectrum analyzer operates by sweeping a wavelength selective device through the desired spectrum to determine the spectral distribution of the intensity. There are mainly three types of optical spectrum analyzer systems: diffraction grating, Fabry-Perot interferometer and Michelson interferometers.

The diffraction grating, diffracts the light in different direction depending on the wavelength and the photo-detector is moved accordingly while sweeping the spectrum

The Fabry-Perot interferometer is based on the etalon which only transmits a single wavelength depending on the distance between the reflecting surfaces.

The Michelson interferometer yields a wavelength dependent interference pattern that can be measured. [18]

3.11. Photodetector

A standard photodiode detects incoming light through absorption of photons. By considering the units of the relevant quantities it is possible to relate the detected signal to the incident light. The incident light will consist of an electric field E . The intensity of the light will be proportional to the electrical field square:

$$I \sim |E|^2 \quad (15)$$

The intensity of the light is power/ area or energy/(area*time):

$$I = \frac{P}{A} = \frac{\varepsilon}{At} \quad \left[\frac{J}{m^2s} \right] \quad (16)$$

As the energy of the light is quantized:

$$\varepsilon = Nh\nu \quad (17)$$

where N is the number of photons, h is Planck's constant and ν is the optical frequency, the intensity of the incident light will be proportional to the number of photons for a given frequency.

The photodetector is normally some form of photodiode where an incident photon excites an electron from the valenceband to the conductance band. The design of the diode provides that the excited electrons induce a current I_c that is proportional to the number of excited electrons. This current is proportional to the induced voltage U , depending on the impedance R of the detector.

$$U = RI_c \quad (18)$$

As a single incident photon will excite a single electron with a probability measured by a constant (quantum efficiency η), as long as the energy of the photon is larger than the bandgap of the photodiode, the induced current will be proportional to the number of incident photons.

Given these relations, the voltage of the signal from the photo-detector will be directly proportional to the intensity of the light and to the square of the electrical field

$$U \sim I \sim |E|^2 \quad (19)$$

3.12. Tunable light source (TLS)

In principle, there are two different methods to vary the wavelength of the emitted light [19] from a TLS. The first method is level tuning, where the energy levels between which lasing occur can be altered through external influence. In semiconductor lasers, the upper and lower constitute the conductance and valence band that can be slightly shifted through temperature, pressure or magnetic field variations.

The second method is cavity tuning, where the amplifying material has broad and continuous energy band. The emitted light is dispersed with a grating and only one wavelength is fed back into the gain medium. A wavelength adjustable external cavity is thus found, and the laser can be tuned rotation the diffraction grating.

It is also possible to alter the wavelength of the light after it is emitted. This can be done with the help of non-linear optics where different wavelengths yield either the sum or the difference wavelength of the initial light. It can also be achieved through Raman scattering, where light interacts with matter to either lose or gain energy from vibrations in the material and thus shift the frequency.

3.13. Erbium-doped Fiber Amplifier (EDFA)

The Erbium-doped fiber amplifier is an optical amplifier using Erbium-doped fibers as gain-medium. The gain is pumped at $\lambda \sim 980$ nm and the spontaneous and stimulated emission is $\lambda \sim 1.5$ μm . The gain spectrum is rather wide as seen in Figure 15 [20] and can amplify at any wavelength over a large spectrum. The EDFA is also homogeneously broadened [21], which means that gain competition will occur between different wavelengths.

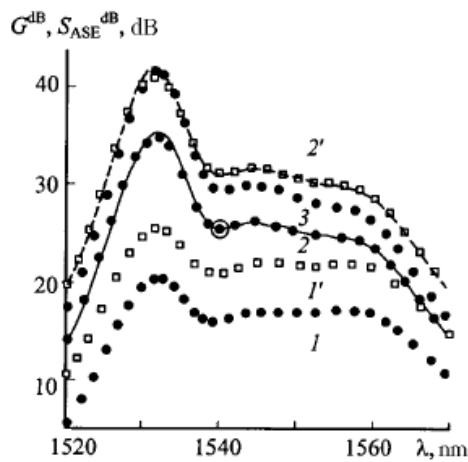


Figure 15. Gain spectrum for Erbium doped fiber amplifier at various pump powers

3.14. Optical Modulator

There are several methods to modulate an optical signal. It can either be by direct modulation of the laser source or by external modulation [6]. The spectrum of the modulated signal will, in its simplest form, consist of an optical carrier with dual sidebands symmetrical around the carrier. The distance between the carrier and the sidebands will correspond to the modulation frequency.

$$\Delta\lambda = \frac{\lambda^2}{c} \Delta\nu \quad (20)$$

thus a 2 GHz modulation corresponds to ~15 pm separation between the optical carrier and the sidebands.

In the proposed setup, a LiNbO₃ Mach-Zehnder modulator is used to transform the microwave signal to the optical domain.

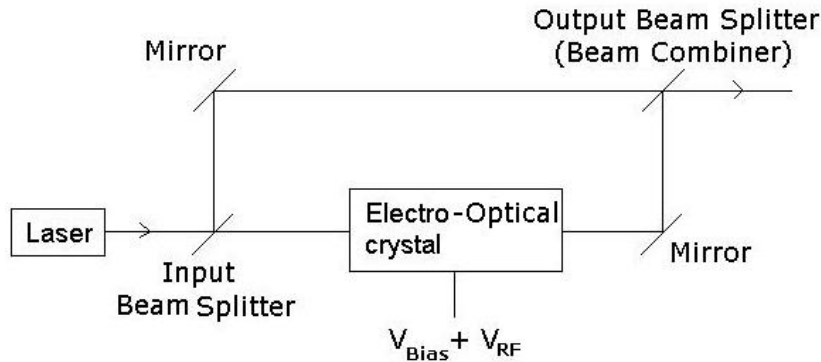


Figure 16. Setup of Mach-Zehnder Modulator

The setup of the Mach-Zehnder modulator uses a Mach-Zehnder interferometer with a controllable optical path length. The incoming light will be divided into two separate parts and then combined again after traversing different paths. If the optical path length of the two arms differ by an odd integer of a half wavelength, $\Delta L = (2n+1)\lambda/2$, the two beams will destructively interfere at the output and the intensity will be zero. If instead the optical path difference is an integer of a full wavelength $\Delta L = n\lambda$, the two beams will instead constructively interfere and the intensity will be maximal. In a standard Mach-Zehnder interferometer there are two reciprocal outputs, thus if the intensity is maximum in one of the outputs it will be minimal in the other and vice versa. However, one of the outputs is often blocked in the modulator. The electro-optical crystal in the setup is a LiNbO₃ crystal which has the property that its refractive index can be altered by applying an external voltage utilizing the Pockel's effect. This changes the phase of one of the arms and equally the optical path difference. Using this, it is possible to control the intensity distribution between the two optical outputs and thus the intensity of the output from the modulator.

The application of the modulator is to modulate a laser beam with a radio frequency of 2-18 GHz. By applying an electrical voltage with the desired radio frequency to the crystal the output optical signal will be intensity-modulated. The bias-voltage ensures that when the RF-voltage is zero, the optical path difference will correspond to minimum in the output intensity. The output intensity of the Mach-Zehnder modulator does not vary linearly with the applied voltage:

$$I \sim \sin^2(\Phi V) \quad (21)$$

and thus, the performance of the modulator can only be considered sufficient in the regions where the relation can be linearized.

3.15. Calculations of Mach-Zehnder Modulator

Consider the light that enters the modulator to have the electrical field

$$E_{in} = A \exp(i\omega t) \quad (22)$$

where A is a constant and ω is the optical frequency. This light is divided into two separate parts and one of the arms is subjected to a time dependent phase-retardation. Thus the electric field at the output will be:

$$\begin{aligned} E_{out} &= E_1 + E_2 = \frac{A}{2} \exp(i\omega t) + \frac{A}{2} \exp(i[\omega t + \Delta\delta + \delta_m(t)]) = \\ &= A \exp(i[\omega t + \Delta\delta/2 + \delta_m(t)/2]) \cos(\Delta\delta + \delta_m(t)) \end{aligned} \quad (23)$$

$\Delta\delta$ is the optical path difference between the two arms that can be adjusted with the bias-voltage. Since this is not time dependent it will be omitted in the following derivations. $\delta_m(t)$ is the time dependent phase shift subjected only to one of the arms.

By assuming that the modulation is a measurable function, it can without loss of generality be considered to be a superposition of sinusoidal functions, provided through Fourier analysis. As these are orthogonal, it is sufficient to consider a single term. Thus if the phase-shift is assumed to be of the form: $\delta_m(t) = \beta \sin(\Omega t)$, where Ω is the RF-frequency, the total electric field at the output will be:

$$E_{out} = A \exp\left(i\left[\omega t + \frac{\beta \sin(\Omega t)}{2}\right]\right) \cos\left(\frac{\beta \sin(\Omega t)}{2}\right) \quad (24)$$

If β is assumed to be small, $\exp(x)$ can be approximated with its Taylor expansion.

$$\exp(x) \sim 1 + x + \frac{x^2}{2} + \dots \sim 1 + x \quad (25)$$

Thus:

$$E_{out} = A \exp(i\omega t) \left[1 + \frac{i\beta \sin(\Omega t)}{2}\right] \cos\left(\frac{\beta \sin(\Omega t)}{2}\right) \quad (26)$$

By using the trigonometric identity: $\sin(x) = [\exp(ix) - \exp(-ix)]/2i$, the expression can be written as:

$$E_{out} = \frac{A}{4} [4 \exp(i\omega t) + \beta \exp(i(\omega + \Omega)t) - \beta \exp(i(\omega - \Omega)t)] \cos\left(\frac{\beta \sin(\Omega t)}{2}\right) \quad (27)$$

From this expression it can be seen that there will be three different frequencies present: Ω , $\omega + \Omega$ and $\omega - \Omega$, corresponding to the carrier frequency and the upper and lower sideband respectively.

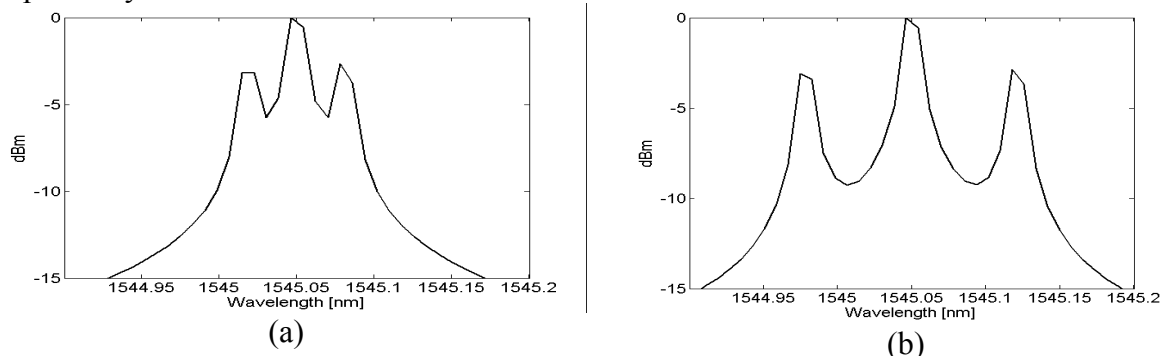


Figure 17. Simulated modulated signal at: (a) 4 GHz, (b) 9 GHz.

4. Fiber Bragg grating (FBG)

The fiber Bragg grating is constructed by introducing a quasi-periodical index modulation of the fiber core that will partially reflect the incoming light.

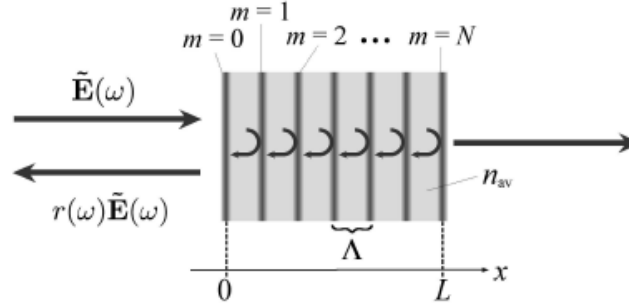


Figure 18. A grating with length \$L\$, period \$\Lambda\$, and an average refractive index \$n_{av}\$ containing \$N+1\$ fringes. Light is incident from the left and partially reflected back determined by reflection coefficient \$r(\omega)\$. [22]

Light incident on the fiber Bragg grating will be partially reflected by every interface between different refractive indices. If the light has a vacuum wavelength that satisfies the Bragg condition:

$$\lambda_B = 2n_{eff} \Lambda \quad (28)$$

all the reflected signals will be in phase at the first interface, regardless of which fringe it was reflected from, as seen in Figure 18. As all the reflections for this *Bragg wavelength* constructively interfere the signal will be reflected in contrast to that of light with any wavelength not fulfilling the Bragg condition. The amount of light reflected at each interface is determined by the Fresnel equation, which for normal incident light is

$$R = \left(\frac{n_1 - n_2}{n_1 + n_2} \right)^2 = \left(\frac{\Delta n}{n_{av}} \right)^2 \quad (29)$$

where \$\Delta n\$ is the modulation depth. As the modulation depth is usually \$\sim 10^{-4}\$ or less, the reflection from each fringe will only be \$\sim 10^{-8}\$.

The periodicity and the strength of the index modulation do not have to be constant throughout the fiber. If the variations are described by a cosine, the refractive index \$n(z)\$ at point \$z\$ will be:

$$n(z) = n_{av} + \Delta n(z) \cos(\kappa(z)z + \varphi(z)) \quad (30)$$

where \$K(z)=2\pi/\Lambda(z)\$ is the spatial frequency, \$\Lambda(z)\$ is the periodicity, or *pitch* of the grating and \$\varphi(z)\$ is a variable phase factor. If \$K(z)\$ is varied over the grating, it is called a *chirped* grating and a varying modulation depth \$\Delta n\$, is called an *apodized* grating.

4.1. Properties of fiber Bragg gratings

One of the key features of a FBG is the complex reflection and transmission coefficient that fully describe how it affects light. These coefficients can be obtained through the so called *coupled-mode theory*. The derivation of the coupled-mode equations and their parametrical solutions are beyond the scope of this thesis and will be omitted, however they can be found in [22,23]. It can be shown [22], that the coupled-mode equations can be analytically solved for two special cases:

1. In the case of very weak gratings, where the transmitted amplitude is unaffected by the reflections. In this case the reflection coefficient and the grating characteristics are directly related by a Fourier transform. In the case of strong gratings, the multiple reflections will affect the calculations and the solution does not appear in a closed form. However, several of the key aspects obtained from the weak grating still apply to the strong gratings.
2. In the case of a uniform grating, where the periodicity of the grating is constant, the coupled-mode equations can be solved in a closed form.

However, it is possible to determine the characteristics of more complicated gratings through numerical simulations. For instance, the Transfer Matrix Method (TMM) uses piecewise, uniform gratings to calculate the reflection coefficients. One can measure directly the reflection or transmission spectra with an optical spectrum analyzer (OSA) once the FBG has been manufactured.

4.2. Variations of fiber Bragg gratings

4.2.1. Chirped grating

By varying the periodicity of the refractive index modulation throughout the grating it is possible to achieve a much broader reflection band. If the variation of the periodicity is small, it can be considered locally uniform. Because of this, each part of the grating will reflect different wavelengths without affecting each other. The resulting reflection spectrum is a much broader but weaker reflection band. To achieve the same strength of the reflection, a much stronger FBG is needed. In Figure 19, the transmission spectra of a 5 cm long grating with and without a 1 nm chirp were simulated at different strength of modulation depth. As seen, the chirp readily broadens the reflection band while significantly reducing the strength.

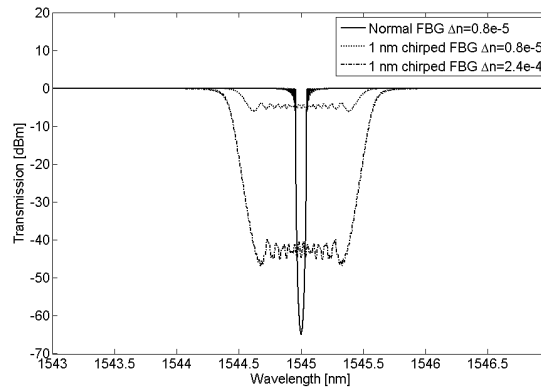


Figure 19. Simulated FBGs with and without chirp at various modulation depths

4.2.2. Apodized grating

In an apodized grating, the modulation depth is varied over the length of the grating. The effects of this can be obtained through Fourier analysis. If the grating characteristics are described by $\kappa(z)$ and its Fourier transform $F\{\kappa(z)\}$, a non-apodized grating can be considered to be:

$$\kappa'(z) = \int_{-\infty}^{\infty} \kappa(z)(\theta(z) - \theta(z - L)) = \int_{-\infty}^{\infty} \kappa(z) \text{rect}(z) \quad (31)$$

The Fourier transform of the non-apodized grating will be:

$$F\{\kappa'(z)\} = \text{sinc}(z) * F\{\kappa(z)\} \quad (32)$$

The sinc-function has several side-lobes in the spectrum which occur due to the sharp edge of the rect-function. By introducing an apodization of the grating, the sharp edges of the grating can be avoided, effectively suppressing the side lobes. Some commonly used apodization profiles are:

1. Cosine: $w(z) = \cos(\pi(z - L/2))$
2. Hamming: $w(z) = 0.54 - 0.46 \cos(2\pi z)$
3. Super Gaussian $w(z) = \exp\left(-\left[\frac{z - L/2}{a_1}\right]^{a_2}\right)$, where a_1 and a_2 are constants.

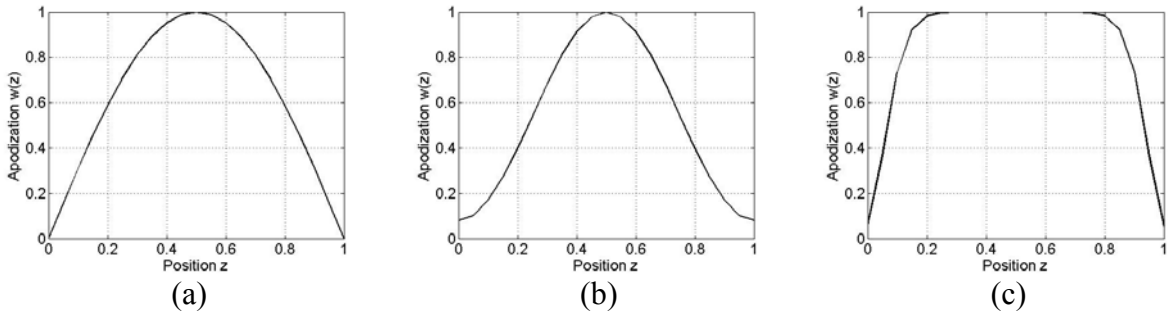


Figure 20. Apodization: (a) Cosine, (b) Hamming and (c) Super Gaussian

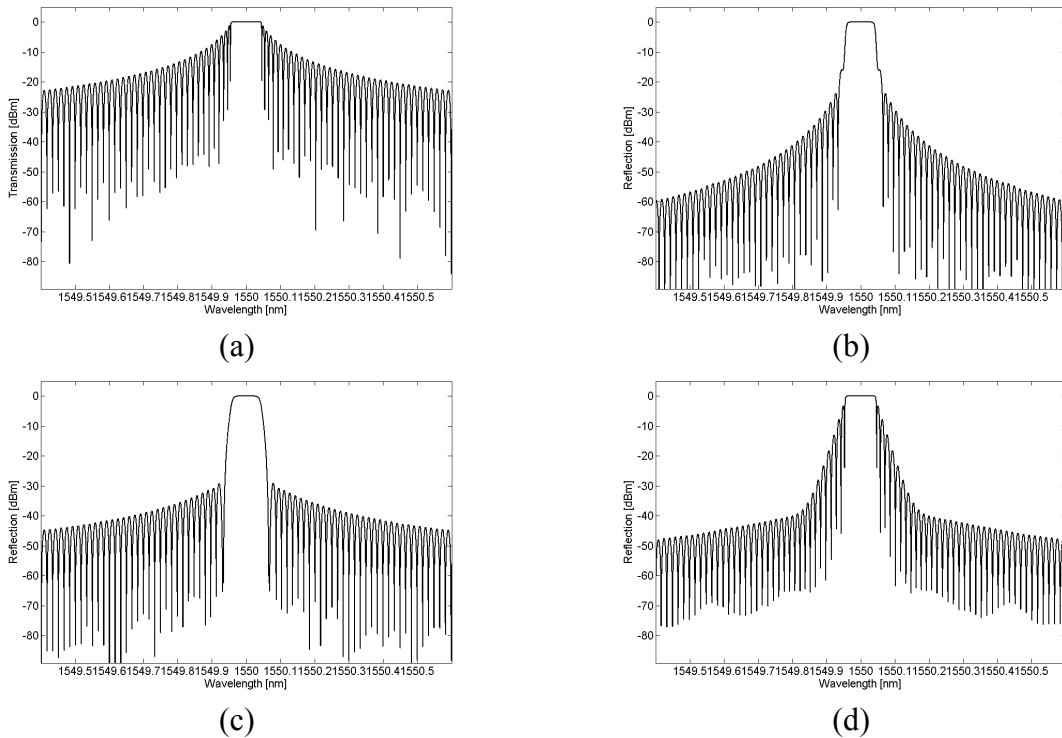


Figure 21. Simulated reflection spectra of a grating with different apodization: (a) No Apodization, (b) Cosine, (c) Hamming, (d) Super Gaussian

As seen in Figure 21, it is clear that all apodization reduces the side-lobes of the not reflection spectra. However it is not readily seen which apodization is optimal as this may vary with the application of the grating.

4.2.3. Phase-shifted FBG

In the expression describing the index modulation in eq. (30), there is a term $\varphi(z)$. This term describes the phase of the index modulation and is usually set to a constant value. However, by introducing a π phase shift in the middle of the grating the result will in effect be two identical gratings, separated by a half wavelength. The consequence of this will be that the two separate grating will act as an extended Fabry-Perot etalon. The reflections from the first half of the grating will be out of phase with the reflections from the second half and will destructively interfere. Due to conservation of energy and momentum, the light will be transmitted instead. However, it will only be a small segment of the reflected spectrum that will be affected and this will open up a very narrow transmission peak in the middle of the reflection band.

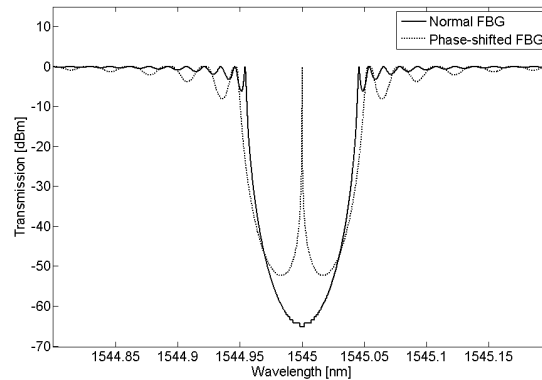


Figure 22. Simulated FBG with and without phase-shift.

4.2.4. Birefringent FBG

Light propagating through a material consists of two orthogonal polarization states. Each of the states represents electromagnetic oscillations along a direction orthogonal to the direction of propagation. For instance, if the light propagates along the z-direction, the TE-polarization may be in the x- and the TM-polarization may be in the y-direction. If the material exhibits different refractive indices along different directions, it is considered birefringent. For instance, if the refractive index in the x-direction is smaller than in the y-direction, the TE-polarization will travel faster than the TM-polarization. The cause of the birefringence can be either intrinsic, geometric or external. Intrinsic birefringence is caused by asymmetric crystal structures in the material, where the atoms or molecules can move more easily in one direction than the others. Geometric birefringence is when the spatial distribution of the material somehow restricts the oscillations of the electromagnetic field differently for the two polarization states. Externally caused birefringence is when some external force or manipulation alters the refractive index asymmetrically. Since the Bragg condition for the FBG is directly proportional to the index of refraction, birefringence will effectively cause the different polarization states to have different λ_B . In the case of a phase shifted FBG, the shift of wavelength can be larger than the FWHM of the transmission peak. Thus it is possible to observe dual peaks as both polarization states are present. In the case of linearly polarized light only a single peak may be visible.

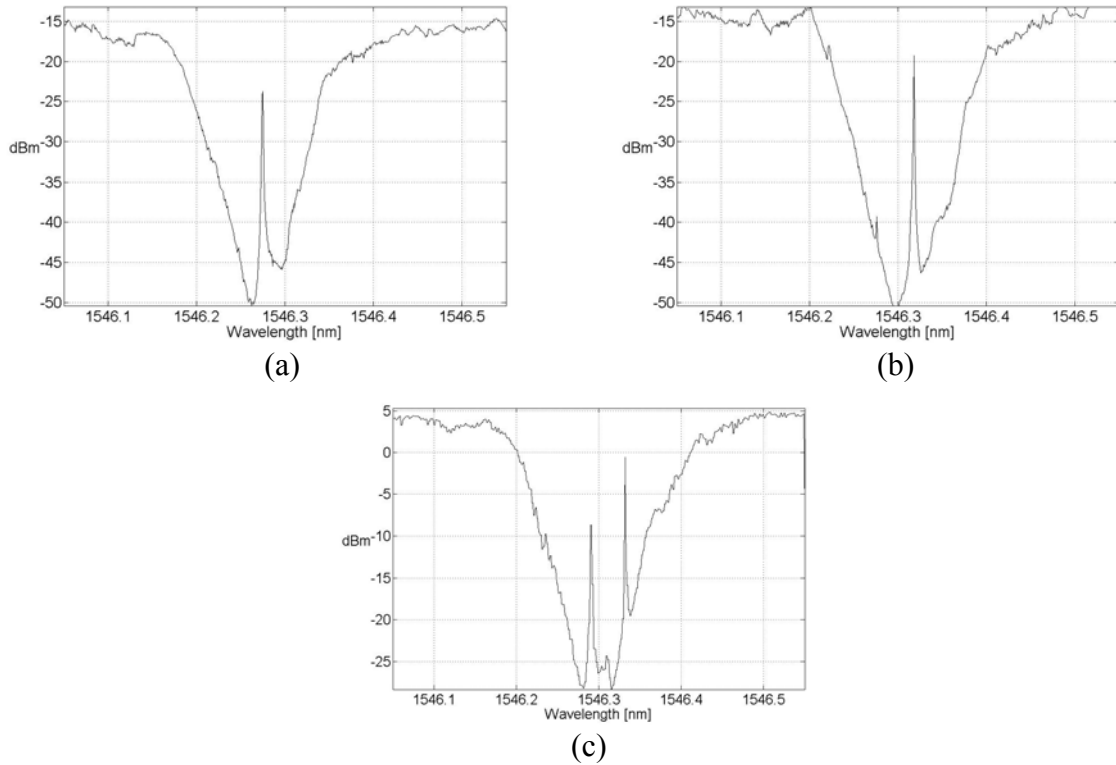


Figure 23. Measured spectrum of birefringent FBG for (a) x-polarization, (b) y-polarization, (c) x- and y-polarization

4.3. Optimizing desired FBG for tunable GHz filter

The intended application of the tunable FBG is to rapidly filter out single sidebands of a modulated optical signal. The principle exploited here is to transmit the chosen sideband through the narrow passband of a DFB grating and reflect the carrier and the unwanted sideband in the stopband of the grating. The grating is chirped to ensure a sufficiently broad stopband. To be able to single out one of the sidebands, the carrier wave needs to be sufficiently suppressed. As the minimum distance between the carrier and the sideband will be ~ 2 GHz, corresponding to 15 pm, the transmission peak needs to be very narrow. Secondly, the maximum distance between the carrier and the sidebands will be ~ 18 GHz, corresponding to 135 pm. In order to always stop the unwanted sideband and carrier, even when the grating is tuned the most, the reflection band needs to be at least four wider than 135 pm to ensure that both sidebands are blocked regardless of the instantaneous spectral position of the transmission peak. Numerical simulations yielded a sufficiently good grating design.

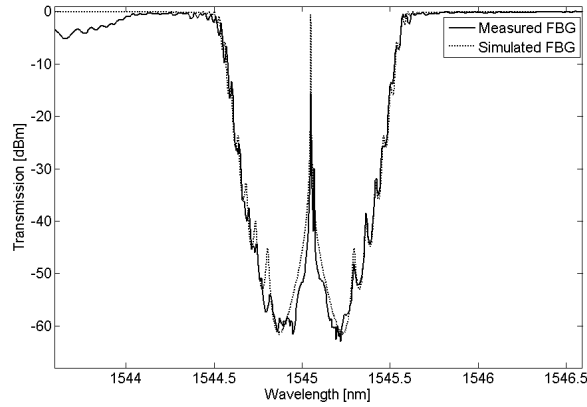


Figure 24. Measured and simulated spectra of phase-shifted FBG

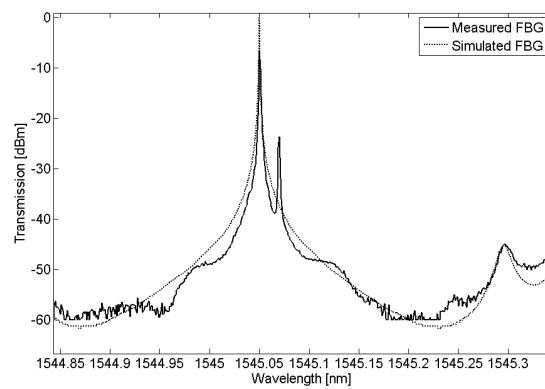


Figure 25. Transmission peak of phase-shifted FBG

The grating in Figure 24 has the following characteristics:

- Grating length: 50 mm
- Chirp: 1 nm
- Phase-shift: π at $L/2$

- Apodization: Super Gaussian $w(z) = \exp\left(-\left[\frac{z - L/2}{0.45}\right]^{10}\right)$

- Modulation depth: $\sim 2 \times 10^{-4}$

5. Tuning fiber Bragg grating

The central wavelength of a FBG is determined by the Bragg condition, in eq. (28)

$$\lambda_B = 2n_{\text{eff}}\Lambda$$

Differentiating this yield:

$$\Delta\lambda_B = 2(n_{\text{eff}}\Delta\Lambda + \Lambda\Delta n_{\text{eff}}) \quad (33)$$

which gives:

$$\frac{\Delta\lambda_B}{\lambda_B} = \frac{\Delta n_{\text{eff}}}{n_{\text{eff}}} + \frac{\Delta\Lambda}{\Lambda} \quad (34)$$

By either varying the pitch, $\Delta\Lambda$, or the refractive index, Δn_{eff} , the central wavelength can be shifted. There are several effects that alter either of the components.

5.1. Altering the pitch of the FBG

The periodicity, or *pitch*, of the grating is simply the distance between the fringes. If the grating has length L with N number of fringes, the pitch will be:

$$\Lambda = \frac{L}{N} \quad (35)$$

Differentiating this yield:

$$\Delta\Lambda = \frac{\Delta L}{N} \quad (36)$$

$$\frac{\Delta\Lambda}{\Lambda} = \frac{\Delta L}{L} \quad (37)$$

Thus, the relative change of the pitch is identical to the relative change of the grating length. This change can either be achieved through tensile stress, by simply stretching the fiber or through thermal expansion. The thermal expansion is determined by:

$$\frac{\Delta L}{L} = \alpha\Delta T \quad (38)$$

where α is the thermal expansion coefficient determined by:

$$\alpha = \frac{1}{L} \frac{\partial L}{\partial T} \quad (39)$$

However, the thermal expansion coefficient for silica is only $\alpha = 5 \times 10^{-7} \text{ K}^{-1}$, which only give a negligible contribution to the shift in wavelength.

5.2. Altering the refractive index of the FBG

The refractive index of the fiber can be either through the photo-elastic effect or the thermo-optic effect. The relative change in refractive index, due to the thermo-optic effect is:

$$\frac{\Delta n_{eff}}{n_{eff}} = \xi \Delta T \quad (40)$$

where ξ is the thermo-optic coefficient:

$$\xi = \frac{1}{n} \frac{dn}{dT} \quad (41)$$

The coefficient for silica is $\xi = 6.5 \times 10^{-6}$ which is an order of magnitude larger than the thermal expansion coefficient in eq. (39). The photo-elastic effect is a response of the refractive index to tensile stress along directions perpendicular to the direction of the propagation of light. If the light propagates along the z-axis, the normal directions will be the x-y-plane. As the light can be polarized along either the x-axis or the y-axis (or any linear combination of these) it is important to note whether the stress is parallel or perpendicular to the polarization direction. Thus, for a non-uniform tensile stress the response will be different for different polarization states. It can be shown that the photo-elastic effect will be [24]:

$$\left. \begin{aligned} \frac{\Delta n_x}{n_{eff}} &= -\frac{n_{eff}^2}{2} [p_{11}\varepsilon_x + p_{12}(\varepsilon_y + \varepsilon_z)] \\ \frac{\Delta n_y}{n_{eff}} &= -\frac{n_{eff}^2}{2} [p_{11}\varepsilon_y + p_{12}(\varepsilon_x + \varepsilon_z)] \end{aligned} \right\} \quad (42)$$

where p_{11} is the photo-elastic coefficient for parallel stress and p_{12} is for perpendicular stress and $\varepsilon_i = \Delta L_i / L_i$ is the directional strain of the fiber. The photo-elastic coefficients are for silica [25]:

$$p_{11} = 0.126$$

$$p_{12} = 0.260$$

It is clear that the photo-elastic effect induces birefringence for asymmetrical stresses, but that a strain in the y-direction still affects the refractive index in the x-direction and vice versa.

5.3. Tuning of metal filled fiber Bragg grating

The component used is a FBG written in a metal filled twin-hole fiber. One of the metal columns is connected to a pulse generator which can deliver short electrical pulses of a few volts. The electrical energy will increase the temperature of the electrode due to the resistive load and will change the refractive index accordingly.

- The heat will cause the electrodes to expand which will induce stresses in the fiber glass that change the refractive index due to the photo-elastic effect
- The heat that dissipates into the fiber core will increase the temperature of the fiber and change the refractive index through the thermo-optic effect.
- The heat in the fiber core will also cause thermal expansion which will change the pitch of the grating.

Since these effects occur simultaneously, numerical simulations are needed to describe the dynamical change in refractive index due to the deposited heat [23].

The effect of the deposited heat is that the Bragg wavelength shifts to longer wavelengths. However, since the applied stress is anisotropic, the process will shift the different polarization directions differently and thus increase the birefringence. After the electrical pulse, it is vital that the FBG is cooled off enough to return to the initial Bragg wavelength. This process can be accelerated by using a Peltier cooling element [26] which allows for higher repetition rates.

6. Rapid optical scan of the microwave spectrum

Rapid scanning of the microwave spectrum, represented by Optical Block 2 in Figure 1 is needed to determine the frequency received i.e., by which the optical carrier has been modulated. The optical signal will consist of a central optical carrier along with two symmetrical side lobes as seen in Figure 17. The distance between the carrier and the sidebands is directly proportional to the modulation frequency as seen in eq. (20). If the wavelength of the optical carrier is known, it is possible to determine the modulation frequency by measuring where the sidebands are. This is done by using a very narrow transmission filter that reflects all wavelengths in the spectrum of interest, except for a narrow transmission peak. The transmission peak is swept through the interesting wavelengths and the output is registered by a photodiode connected to an oscilloscope. If there is a RF-signal and thus sidebands, the photodiode will detect a signal when the transmission peak overlaps the wavelength of the sideband. Since the speed of the filter is known (or at least can be determined), the time it takes between the beginning of the sweep and the signal is detected can be directly correlated to the modulation frequency. Note that the photodiode does not have to be particularly fast since it integrates the microwave signal. A low noise, limited bandwidth photodiode can be used.

6.1. *Suppression of optical carrier*

The signal that is analyzed is composed by a strong optical carrier with two weaker sidebands besides it. As the detector is a photodiode that simply registers the intensity of the incident light, it does not discriminate between the carrier and the sidebands. If the carrier is not sufficiently suppressed, the photodiode will not only detect the sideband but also the partially suppressed carrier. Thus, a few methods using phase-shifted FBGs to suppress the optical carrier were examined.

6.1.1. Double pass through transmitting fiber Bragg grating

The phase-shifted FBG used has a relatively wide reflection band with a narrow transmission peak in the center. By allowing the signal to pass through the filter twice, the filtering effect is significantly improved. Since the transmission of the peak is nearly 100 %, the corresponding wavelength will ideally not be affected by a second pass. However, the regions that are reflecting will suppress the signal twice.

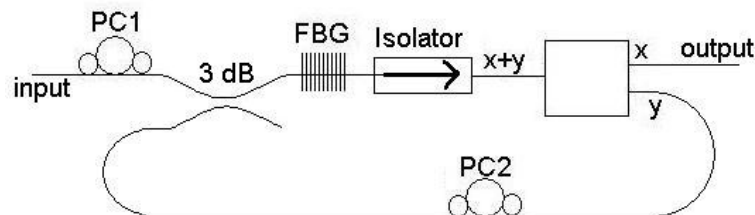


Figure 26. Setup for dual pass of fiber Bragg grating

One way of achieving dual pass of the fiber Bragg grating can be seen in Figure 26. The incoming light is aligned with the y-axis with the first polarization controller (PC1). Thus, the light passes through the FBG and exits the polarization splitter through the y-branch. A second polarization controller (PC2) is used to rotate the polarization along the x-axis. As the light passes through the FBG a second time, it will exit through the x-branch of the polarization splitter. The isolator is needed in order to suppress the reflected light which otherwise could propagate through the loop in the wrong direction. Since the double pass

requires several different components in series, each introducing a slight loss of signal, the overall loss will be larger than for a single pass through only the FBG.

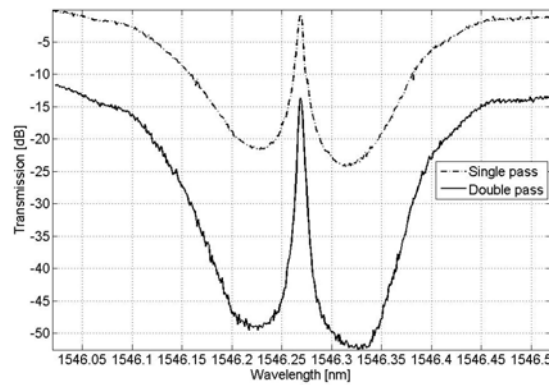


Figure 27. Transmission spectra from single- and double pass of phase-shifted FBG

However, the dual pass requires a non-birefringent FBG since each of the passes are at different polarization states. If the index of refraction is different for the different polarization states, the position of the transmission peak will be different and the filters will not overlap. In Figure 28, the phase-shifted FBG is birefringent and the suppression is not doubled. However, the FWHM of the transmission peak is significantly reduced.

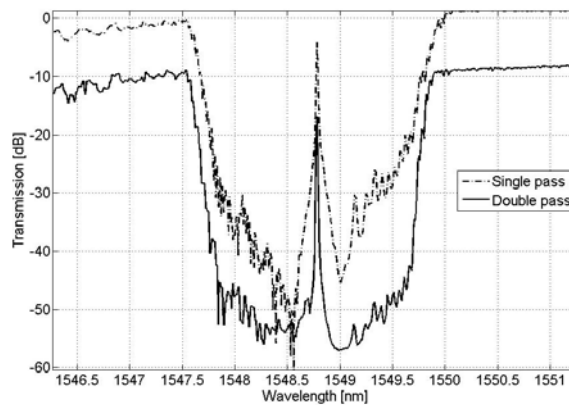


Figure 28. Transmission spectra of double pass of birefringent FBG

The modulated signal filtered twice through the FBG can be seen in Figure 29.

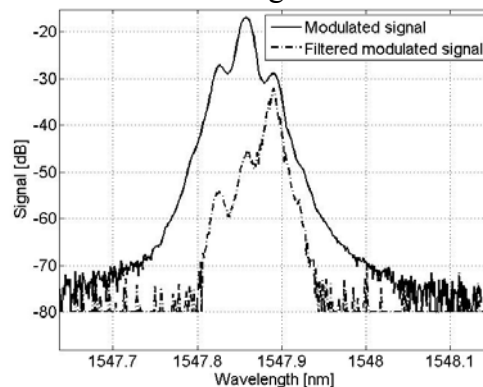


Figure 29. 4 GHz Modulated signal, filtered by double pass through birefringent FBG

6.1.2. Additional suppression of the optical carrier using two very similar FBGs

As the effect of the dual pass requires a non-birefringent fiber, its applications are limited. A method to circumvent this requirement could be to utilize two identical FBGs in series with an optical isolator in between. However, since the FWHM of the transmission peaks are less than 10 pm wide, the precision needed is significant. As the spectrum is to be scanned, both of the FBGs need to be shifted simultaneously and with great accuracy. As the temperature drift is ~ 11 pm/K, even a small variation between the two gratings will greatly reduce the combined transmission.

An alternative to this could be to use two almost identical phase-shifted FBGs which central wavelengths are adjacent but not identical. The first FBG is used in transmission and selectively transmits only the upper sideband, while reflecting a large portion of the adjacent wavelengths. The second FBG is used in reflection where the transmission peak is centered at the carrier wavelength. As it will transmit most of the carrier while reflect most of the adjacent wavelengths, the carrier will be further suppressed while the upper sideband will be virtually unaffected.

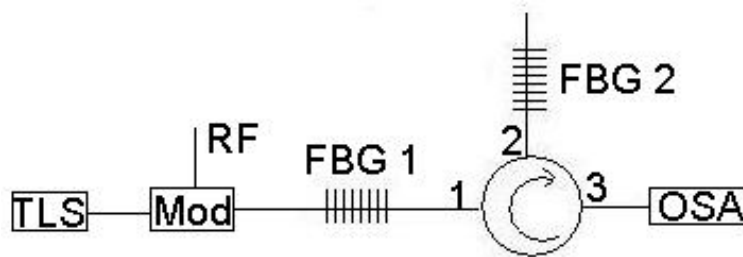


Figure 30. Setup for using one grating in transmission and one grating in reflection

The spectrum of FBG1 and FBG 2 can be seen in Figure 31.

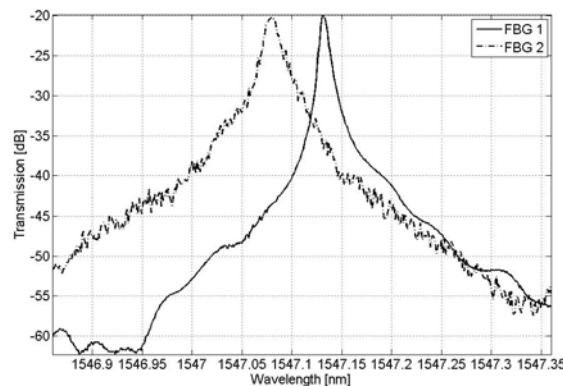


Figure 31. Transmission spectrum of FBG1 and FBG2 from Figure 30

Note that FBG 1 and FBG 2 in Figure 31 are similar phase-shifted FBGs as in Figure 28 but zoomed in on the transmission peak. As FBG 2 is used in reflection, the joint spectrum of FBG 1 and FBG 2 will be:

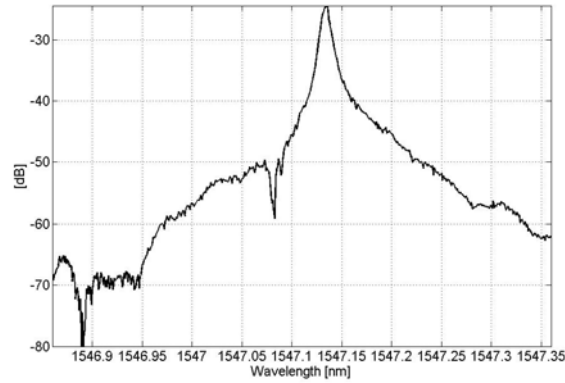


Figure 32. Measured spectrum with FBG 1 in transmission and FBG 2 in reflection

By positioning the optical carrier at the wavelength corresponding to the transmission peak of FBG 2, i.e. at the dip of the joint spectrum, the optical carrier will be suppressed. As the two gratings are independent, it is possible to shift only FBG 1 in order to alter the distance between the peaks.

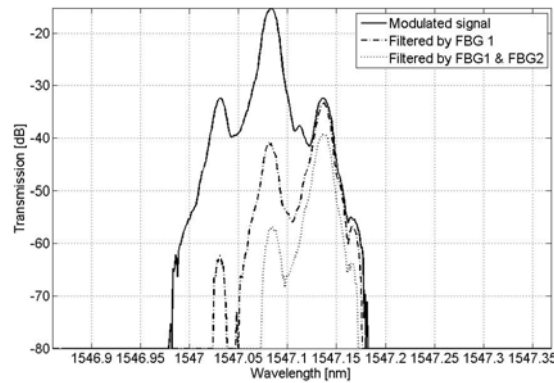


Figure 33. Modulated signal filtered by FBG 1 or FBG 1 + FBG 2

It can be seen from Figure 33 that the reflecting FBG greatly suppresses the optical carrier with small influence on the sideband.

6.1.3. Single sideband filtering using ultra-narrow phase-shifted FBG

The previous methods in section 6.1.1 and 6.1.2 were used in order to improve the performance of existing FBGs. However by manufacturing a novel grating design with internal electrodes for tuning, it was possible to achieve a transmission peak with a FWHM of less than 1pm (i.e., 130 MHz), as seen in Figure 25. The measurement was done by modulating the light from the TLS, filter it with the phase-shifted FBG and detecting it with the optical spectrum analyzer.

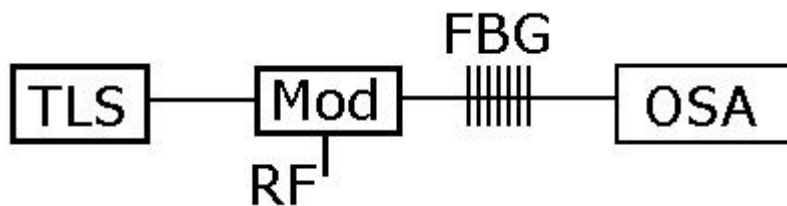


Figure 34. Schematic setup for measuring suppression of optical carrier for phase-shifted FBG

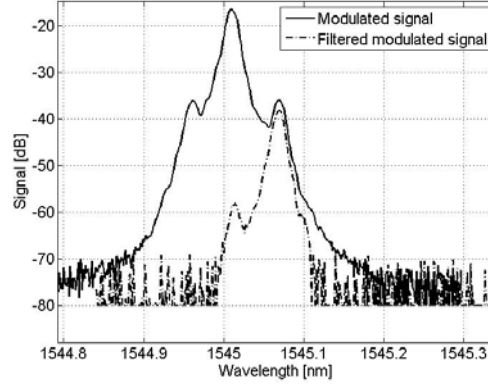


Figure 35. Modulated signal before and after filtering by phase-shifted chirped FBG shown in Figure 24.

The phase-shifted FBG in Figure 35 overlaps the upper sideband of a frequency modulated carrier. It is evident that the filter effectively suppresses the carrier and the lower sideband while transmitting the upper sideband.

6.2. Setup for determining the RF-frequency of a modulated optical signal

The signal to be detected is a RF-signal with frequencies in the range $\Delta\nu = 2-18$ GHz. As the RF-signal is used to modulate an optical carrier generated by a tunable light source, the output is two symmetrical sidebands around the optical carrier. The optical carrier is kept at a constant wavelength λ_0 . The distance between the optical carrier and the sidebands is directly proportional to the modulation frequency as seen in eq.(20)

$$\Delta\lambda = \frac{\lambda^2}{c} \Delta\nu$$

Thus, the sidebands will be located at:

$$\lambda_{SB} = \lambda_0 \pm \Delta\lambda \quad (43)$$

The measurement is done by positioning the transmission peak of the FBG at the wavelength that corresponds to the lower sideband at maximum modulation frequency, i.e.

$$\lambda_{Min} = \lambda_0 - \Delta\lambda_{max} \quad (44)$$

where $\Delta\lambda_{max} = 135$ pm. The sweep is achieved by heating the internal electrodes of the fiber with a short electrical pulse which shifts the Bragg wavelength of the grating to longer wavelengths. After the pulse, the deposited heat will shift the grating to a maximum wavelength corresponding to the minimum modulation frequency

$$\lambda_{Max} = \lambda_0 - \Delta\lambda_{min} \quad (45)$$

where $\Delta\lambda_{min} = 15$ pm. The RF measurement can be performed during this faster phase of heat deposition, or during the slower process of heat removal. The heat dissipates from the fiber and the system slowly cools off which shifts the grating to shorter wavelengths. By doing this, the transmission peak will move from λ_{Max} to λ_{Min} and if there is a sideband at any of the intermediate wavelengths it will only be transmitted when the transmission peak overlap. After a while, all the heat will have dissipated and the grating will have return to its initial wavelength at λ_{Min} , whereupon the sweep can be repeated. Either of these can be blanked in the oscilloscope, so that the apparent frequency sweep always takes place in the same direction, for example from high to low frequency.

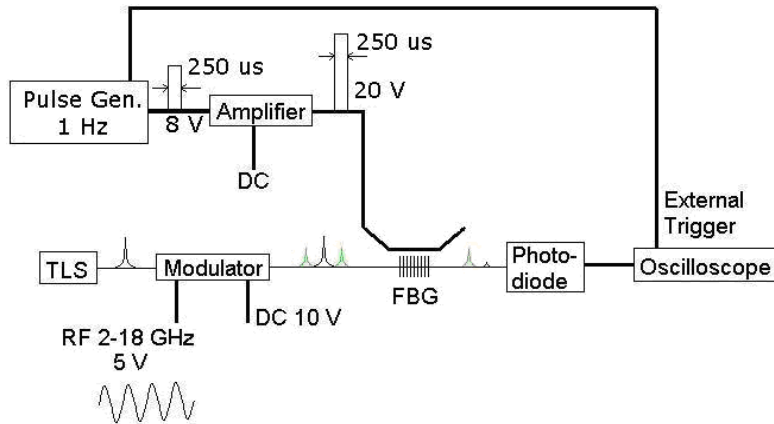


Figure 36. Schematic setup of rapid single sideband measurement

The measurement setup is shown in Figure 36, where the optical signal was generated by the TLS, modulated with a RF-signal from a signal generator, filtered by the FBG and then detected by a photodiode. The photodiode, which registers the intensity of the light, was connected to an oscilloscope to determine at what time after the beginning of the sweep a signal was registered. The oscilloscope was externally triggered by the electrical pulse generator so that the measurement was synchronized with the electrical pulse. The pulse generator yields a short electrical pulse that is amplified and fed into the internal electrodes of the FBG. The slow repetition rate of the pulse generator ensures that the deposited heat is fully dissipated between the pulses.

6.3. Thermal stability of system

A standard fiber Bragg grating shifts ~ 11 pm/ K as seen in Figure 37. However, an FBG in a metal-filled twin-hole fiber that is fixed on an aluminum substrate, shifts ~ 37.6 pm /K [23]. As the sweeping of the FBG-filter is achieved by rapidly changing its temperature, it is important that all deposited heat is extracted before the next pulse is applied. Otherwise, the heat will accumulate and the entire sweeping spectra will shift. The most straightforward method to achieve this would be to use an active cooling system using a Peltier element. Alternatively, if it were possible to measure the drift in wavelength that the phase-shifted FBG is subjected to, the carrier wavelength could be shifted accordingly. In either case, it is necessary to isolate the system to reduce the external influences that could affect the measurements.

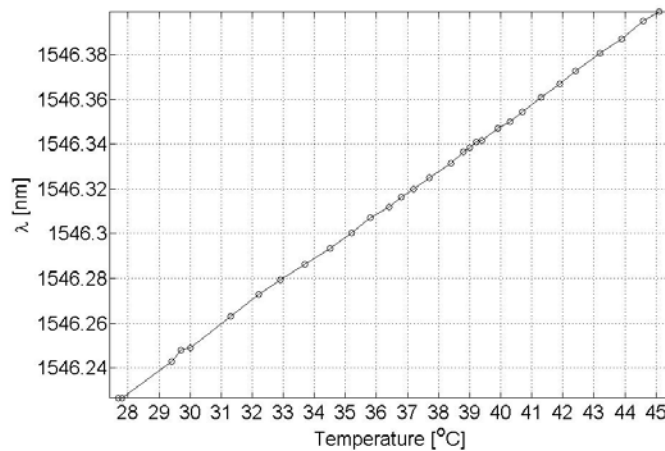


Figure 37. Measured temperature dependence of fiber Bragg grating using a heating element.

6.4. Results

It was not possible to perform a measurement of the full radar spectrum of $\nu = 2-18$ GHz, since the available optical modulator was limited at 10 GHz. Thus, the filter was initially situated at a wavelength corresponding to $\nu \sim 10$ GHz. When the electrical pulse was initiated, the frequency filter would rapidly sweep the spectrum from $\sim 10-2$ GHz due to the heat deposited by the pulse. After the pulse ceased the heat will eventually dissipate and the filter returns to its initial spectral position and thus sweeps the spectrum once again but in opposite direction 2-10 GHz. The rapid sweep due to heat deposition in the electrodes can be seen in Figure 38. In Figure 38 (b), the values have been normalized in order to accentuate the time-variation of the filter. As seen in Figure 39, the sweeping of the spectrum is nearly linear apart from the last region where the filter approaches 2.5 GHz. When the filter reached its maximum temperature in this region, the sweeping will naturally be slowed down. As the filter has reaches its maximum temperature, it will eventually cool off. Heat then dissipates and the sweep is reversed, as seen in Figure 40 (a). The time dependence of the peaks from the cooling of can be seen in Figure 40 (b) and it is clear that it is far from linear. As the process is given by heat conduction, it is reasonable to assume that the time dependence is exponential. The measurement requires that the heat in the fiber fully dissipates after the pulse so that the filter has time to return to its initial wavelength, and thus the repetition frequency was very low ~ 0.5 Hz.

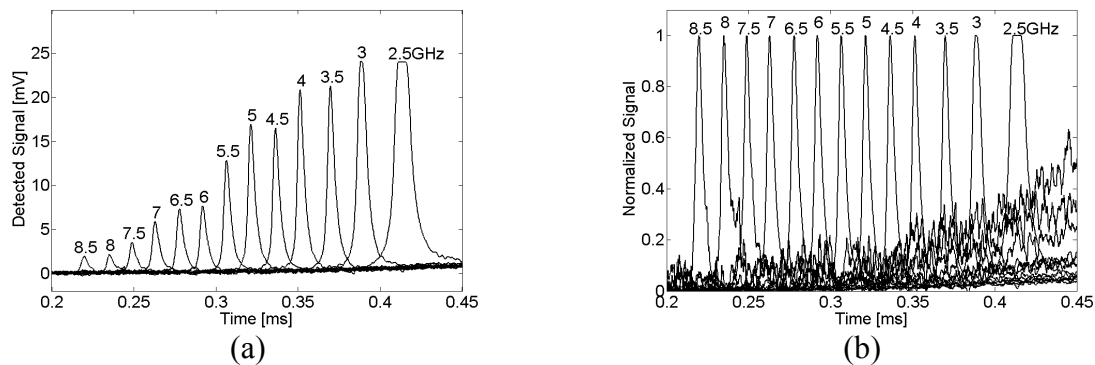


Figure 38. (a) Detected single sideband at different modulation frequencies during rapid sweep of metal-filled FBG filter due to heating from 2.5-8.5 GHz, (b) Normalized values of detected signal

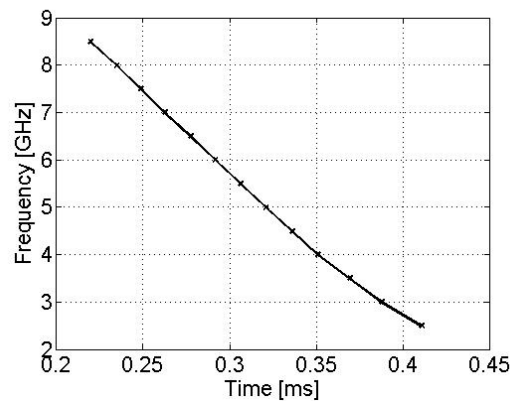


Figure 39. Time dependence of peaks from Figure 38

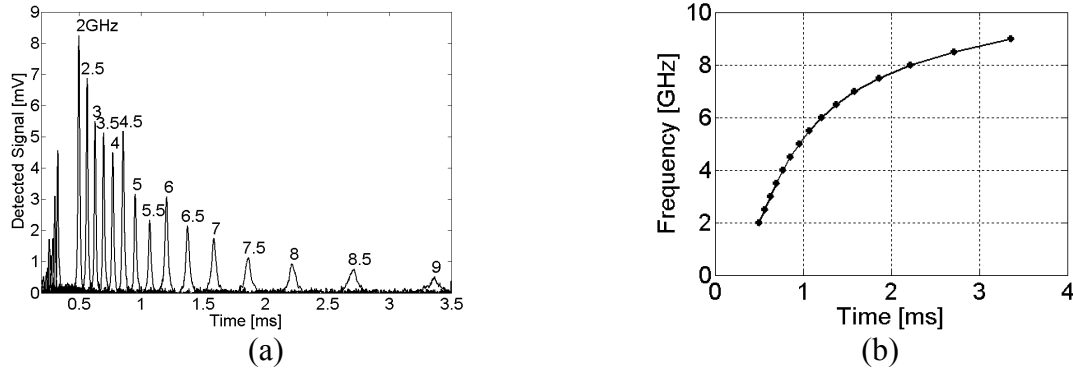


Figure 40. (a) Detected single sideband at different modulation frequencies during slow sweep of metal filled FBG filter due to cooling, (b). Time of detection of the signals at different modulation frequencies.

6.5. Conclusion

The novel tunable fiber Bragg grating developed for this thesis has proven to successfully measure microwave frequency using optical components. The spectrum that could be covered was $f=2.5-8.5$ GHz within 0.2 ms. The limitations in the equipment prevented a scan of the full spectrum 2-18 GHz as the optical modulator was limited at 10 GHz. This limitation can be circumvented by using a faster, more expensive modulator which covers the entire spectrum.

The speed of the sweep is limited by how fast the heat can be deposited in the internal electrodes of the fiber. As the pulse generator that was used was only able to deliver a maximum voltage of 8 V that could be amplified to a maximum of 20 V with available equipment it was not possible to deposit the necessary heat in less than 0.35 ms. However, by using other electronics that can yield high-voltage sub-microsecond pulses, it would be possible to sweep the filter through the microwave spectrum in a much faster fashion. Response times that are less than 10 ns have been reported in similar components [26].

The repetition frequency of the measurements is limited by how fast the heat dissipates after the pulse subsides. As this depends on the temperature and heat conductivity of the surrounding material it can be improved by using either an active cooling or highly heat conductive material.

In either case it is vital that the carrier wavelength is kept at a constant wavelength. If the carrier wavelength would drift ever so slightly, the shift of the microwave spectrum would be significant.

7. Microwave generation using tunable phase-shifted FBG

It is possible to generate microwave signals from the optical domain by beating two optical signals that are adjacent in wavelength. If two optical signals are incident on an optical detector, the registered intensity will consist of not only the original frequencies, but also the sum and difference frequency. As the optical frequency is too high to be detected, this will be averaged to zero which gives a DC contribution to the intensity. However, the difference frequency can be detected if the two optical signals are close to each other in wavelength. The difference in wavelength is related to the difference frequency as seen in eq. (20). This can be achieved by utilizing two separate laser sources [10]. However, in order to obtain a low phase noise, a high quality microwave reference signal is required [11,12]. Another option is to use a single laser, operating at two different wavelengths that are situated spectrally very close to each other. Precise filtering is required that only allows the two wavelengths to lase as well as sufficient gain for both wavelengths. The filtering can be achieved through a Fiber Bragg Grating (FBG) with a wide stopband with two narrow transmission peaks in the middle [13,14,15]. To be able to achieve a stable beating frequency, it is vital that the two optical wavelengths lase simultaneously. However the commonly used erbium-doped fiber amplifier (EDFA) has a homogenously broadened gain spectrum that cause the different wavelengths to compete for the gain. Normally only a single wavelength will lase and suppress the gain for all other wavelengths. In order to avoid this, one can stabilize the system using by introducing some special scheme such as four-wave mixing in a bismuth-oxide fiber [27]. Another option is to use an inhomogeneous broadened gain medium such as a semiconductor optical amplifier (SOA) where the competition between different wavelengths is not as strong [28]. The proposed method only uses EDFAs along with the special tunable FBG to sustain dual-wavelength operation for microwave generation and allow for higher power signal generation.

7.1. Setup for polarization-split cavity for dual wavelength operation

The Erbium-doped amplifier suffers from homogenous broadening. Because of this, if one wavelength begins to lase, it will deplete the gain and prevent the other wavelength from lasing. However, the issue can be circumvented by utilizing two independent EDFA, each one amplifying one wavelength. The setup in Figure 42 consists of two parts; the mutual filtering loop and the amplifying loops. The two parts are joined by a polarization splitter. The filtering loop consists of a birefringent, phase-shifted FBG in transmission and a standard FBG in reflection that is matched to the same wavelength.

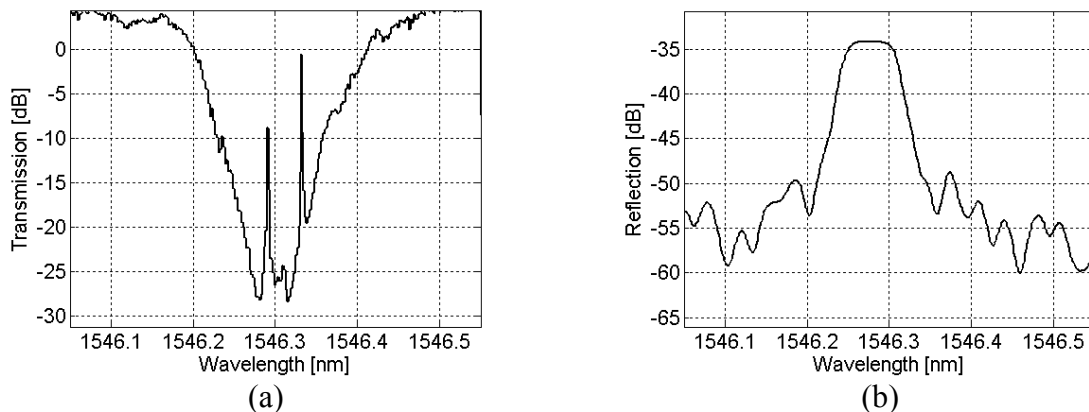


Figure 41 (a) Transmission spectrum of phase-shifted FBG. (b) Reflection spectrum of FBG

The two peaks in Figure 41 (a) are due to the birefringence of the fiber which appears due to the internal electrodes of the fiber. This makes the two polarization states to experience different Bragg wavelengths and thus two peaks appear at different wavelengths. The reflective FBG can be shifted by controlling its temperature and thus it is possible to match both peaks simultaneously.

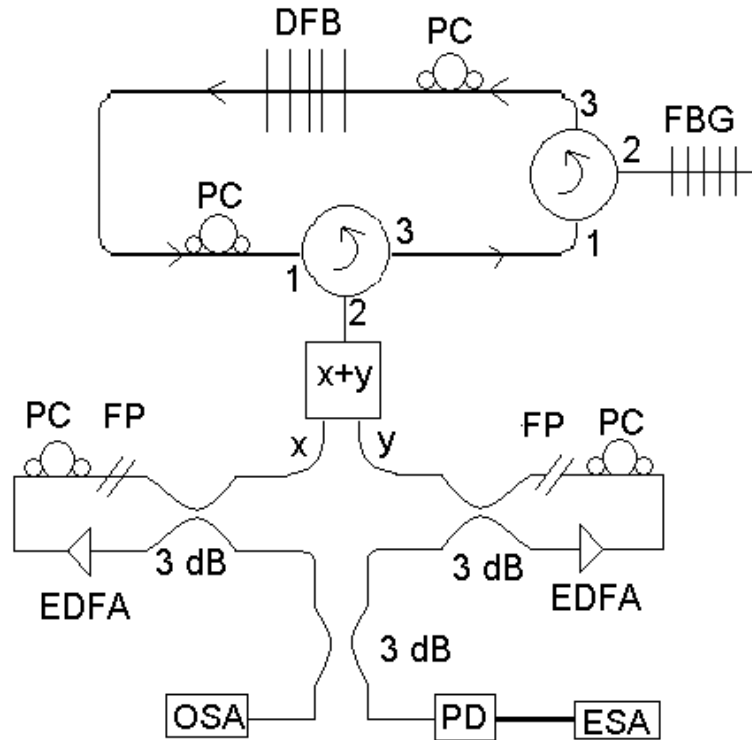


Figure 42. Setup of polarization split cavity

The system will consist of two fiber ring lasers that operate with two orthogonal polarization states at different wavelengths. The ring laser requires several round-trips during which the phase-shifted FBG only transmits a single wavelength for either polarization state. As the light reaches the polarization-splitter, each polarization state enters different arms and is amplified independently. As the output of the laser is directly after the EDFAs, it is necessary to employ Fabry-Perot bandpass filters to suppress the wide unwanted emission spectra of the EDFAs which would otherwise reach the detectors. The reflecting FBG is used to further suppress the irrelevant wavelengths. The output is obtained after the EDFAs and is joined in either an OSA to obtain the optical spectrum or in a photodiode to generate and detect microwave beat signal. The four polarization controllers (PC) are required to ensure that the each polarization state enters the same amplifier every round trip.

7.2. Time-varying optical microwave generation

The wavelength-selective component of the dual-wavelength ring-laser in Figure 42 is the birefringent, phase-shifted FBG. The beat frequency, generated at the photodiode is proportional to the wavelength distance between the two incident signals. By varying the distance between the peaks, it is possible to vary the beat frequency accordingly. As the component is installed with internal electrodes, it is possible to shift the grating with an externally applied electrical voltage. The temperature dependence of the component can be seen in Figure 43:

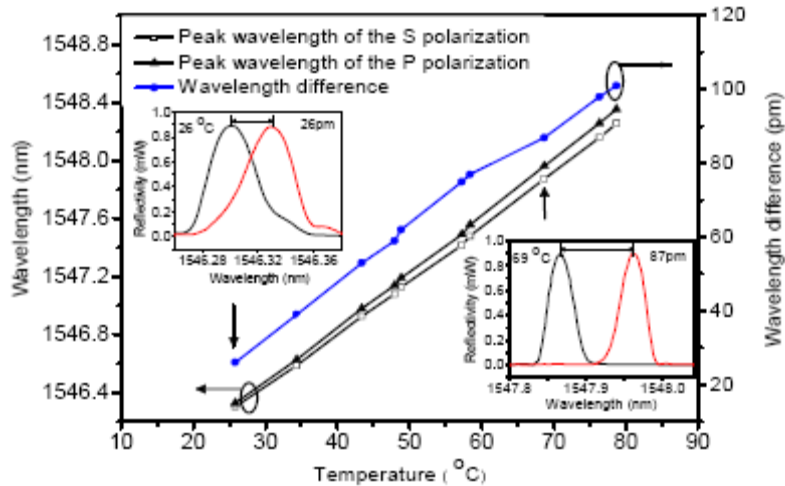


Figure 43. Temperature dependence of Bragg wavelength for S- and P-polarization in a steady state situation [16]

As the internal electrodes have a low melting point (described in section 3.3), the applied voltage is very low to avoid breakage of the component. The electrical pulse was a saw-tooth function with a peak value of 2 V and a frequency of 2 mHz, i.e. a period length of 500 s. The low frequency was required because the electrical spectrum analyzer could only save a measurement every 8 seconds. The sawtooth function of the applied voltage can be seen in Figure 44.

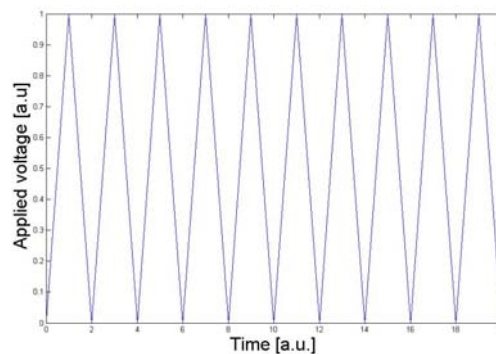


Figure 44. Time-varying electrical voltage

7.3. Results

By correctly adjusting the polarization controller, it was possible to separate the two polarization states in different amplifiers and successfully maintain dual-wavelength operation.

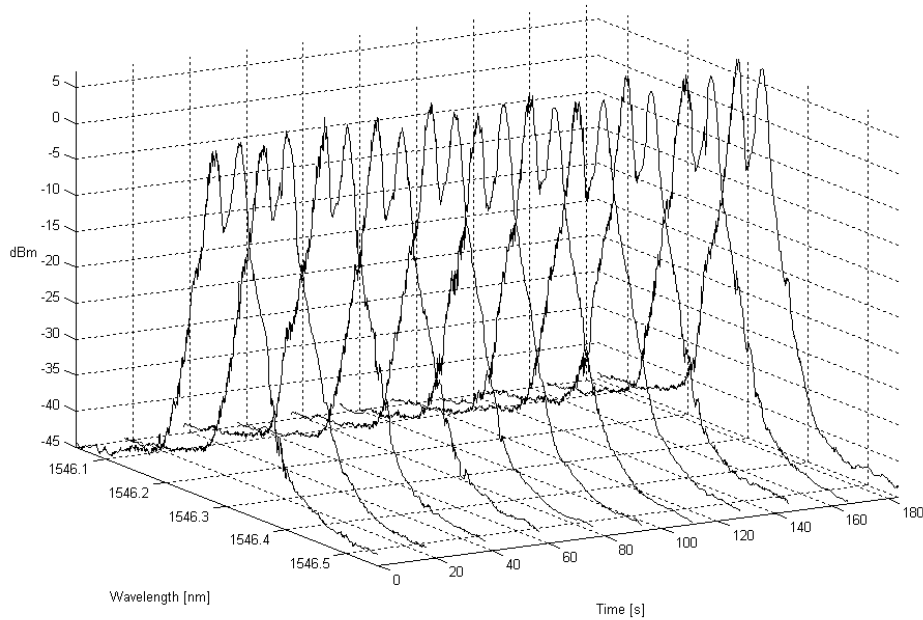


Figure 45. Dual-wavelength operation of polarization-split cavity

The output from the ring cavity was registered by the OSA and the spectra can be seen in Figure 45 and it is clear that the two wavelengths lase simultaneously.

7.3.1. Static measurements

The beat frequency was measured at constant temperature without any electrical load on the internal electrodes of the fiber. The results can be seen in Figure 46.

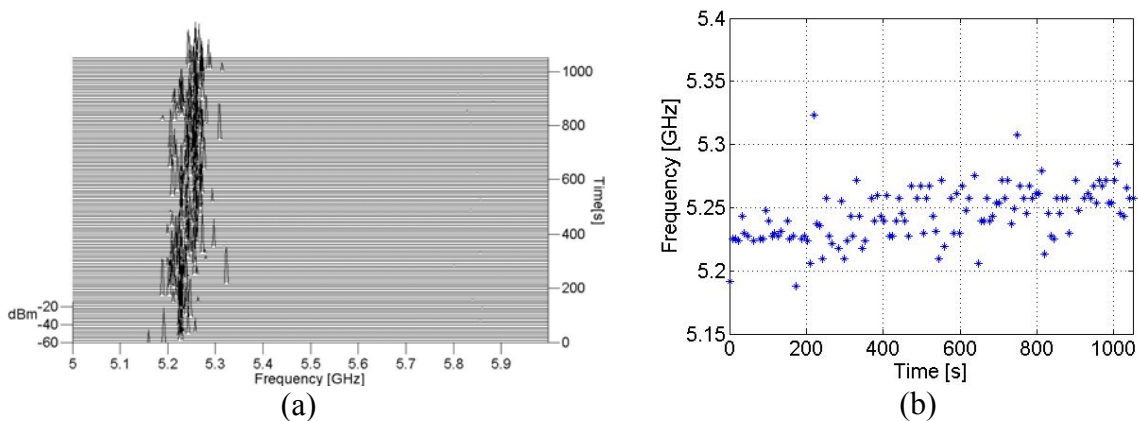


Figure 46 (a) Beat frequency from dual-wavelength operation (b) Time dependence of beat frequencies (above threshold: -55 dBm).

The figure shows both a 3d plot with the intensity of the detected beat frequencies as well as a 2d plot with only the peak values above a certain threshold level. It can be seen that the beat frequency fluctuates slightly over time, approximately ± 50 MHz. This corresponds to $\Delta\lambda \sim 0.4$ pm in variation of the optical wavelength.

7.3.2. Time-varying measurements

The time-varying beat frequency was achieved by applying a slow varying electrical ramp-function with a low voltage to the internal electrodes of the fiber. The frequency of the ramp-function was set to ~ 2 mHz and the voltage varied between 0-2 V. The result can be seen in Figure 47. In this figure, the slight fluctuations of the beat frequency are also visible but are not as pronounced. It is clearly visible that the beat frequency follows the applied voltage with a period of $\tau \sim 500$ s.

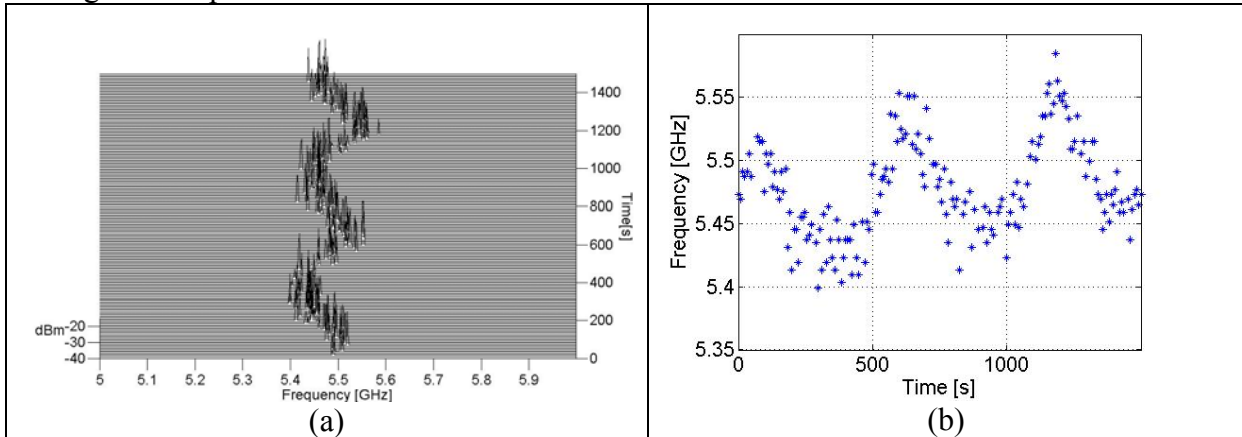


Figure 47 (a) Beating frequency from dual-wavelength operation with a 2 V ramp-function at frequency 2 mHz, applied to electrodes. (b) Time dependence of beat frequencies (above threshold: -55 dBm).

7.4. Conclusion

The novel configuration for a polarization split cavity provided stable dual-wavelength operation for intervals of time. As the selective FBG filter was electrically tunable, it was also possible to tune the beat frequency of the output. Tuning of the beat frequency requires a change in the wavelength difference between the lasing signals, so the birefringence of the FBG needs to be altered. By applying the electrical signal to the electrodes it is possible to induce an anisotropic stress in the fiber which increases the birefringence. The effect is that the Bragg wavelength for both polarization states increases in wavelength but one of the states increases more rapidly. The dual-wavelength operation requires some time to reach steady-state operation, as the light needs to traverse the cavity in several roundtrips. Since the cavity length exceeds 50 m the roundtrip time will be more than $2.5 \mu\text{s}$. The DC bias to the device available was limited to 2 V, corresponding to a current of approximately 40 mA. This is significantly less than the current bias that similar devices can be subjected to, but since only a single device was available for this experiment, this low current limit was respected. However, experiments have shown that if the FBG were kept at a constant high temperature, below the melting point of the electrodes, the birefringence, and thus the separation of the peaks would increase as seen in Figure 43.

8. General Conclusion and Future Work

Tunable phase-shifted fiber Bragg grating has successfully been used to both generate microwave signals as well as to measure microwave frequencies. The microwave generation was able to generate fairly stable ~ 5.5 GHz microwave signals that could be tuned ~ 100 MHz. The generated frequency is determined by the level of birefringence in the fiber and altering it allows tuning of the frequency. The stability of the system could be improved by reducing the cavity length. A simpler arrangement that could be implemented is to pump two pieces of erbium doped fiber separated by a FBG with a single pump, instead of the commercial optical amplifiers used. The tunability could be increased by applying a much higher voltage to the fiber electrodes.

The frequency measurement was able to successfully measure microwave frequencies in the range 2.5-8.5 GHz. The lower limit could easily be altered by adjusting the initial spectral position of the filter. However, to increase the upper limit of the frequency range requires both a faster modulator as well as a larger applied voltage. The improved modulator is needed to be able to transform the higher frequencies to the optical domain and the higher voltage is needed to be able to sweep the filter over a larger spectra. The speed of the sweep is limited by the time taken to deposit the required amount of energy to scan the filter. By using a much shorter pulse, with much higher instantaneous voltage it should be possible to achieve the same spectral shift in a much shorter period of time. The low repetition rate ensured that the deposited heat was able to fully dissipate between each electrical pulse. However by using active cooling element it should be possible to significantly increase this rate.

References

- 1 J. Capmany, B. Ortega and D. Pastor, "A Tutorial on Microwave Photonic Filters", *Journal of Lightwave Technology*, Vol. 24, No. 1, Jan. 2006
- 2 J. Capmany, J. Mora, B. Ortega and D. Pastor, "Microwave photonic filters using low-cost sources featuring tunability, reconfigurability and negative coefficients", *Optics Express*, Vol. 13, No. 5, pp 1412-1417, Mar. 2005
- 3 I. Jaeger, J Stiens, G. Koers, G. Poesen and R. Vounckx "Hadamard speckle reduction for millimeter wave imaging" *Microwave and Optical Technology Letters*, Vol. 48, No. 9, Sep. 2006
- 4 A. Wiberg, "Generation, Modulation, and Detection of Signals in Microwave Photonic Systems", *Doctoral Thesis in Microtechnology and Nanoscience*, Chalmers, Sweden, 2008
- 5 E. Ackerman, "Broadband linearization of a Mach-Zehnder electro-optic modulator", *IEEE Trans. Microw. Theory Tech.*, Vol. 47, No. 12, pp. 2271-2279, Dec. 1999
- 6 C. Cox, L. Johnson and G. Betts, "An analytical and experimental comparison of direct and external modulation in analog fiber-optic links", *IEEE Trans. Microw. Theory Tech.*, Vol. 38, No. 5, pp. 501-509, May 1990
- 7 Linh V. T. Nguyen and David B. Hunter, "A photonic Technique for Microwave Frequency Measurement", *Photonics Technology Letters*, Vol. 18, No. 10, May 2006
- 8 Xihua Zou and Jianpin Yao, "An optical Approach to Microwave Frequency Measurement With Adjustable Measurement Range and Resolution", *Photonic Technology Letters*, Vol. 20, No. 23, Dec. 2008
- 9 Junqiang Zhou., Songnian Fu, Perry Ping Shum, Shee Aditya1, Li Xia, Jianqiang Li, Xiaoqiang Sun and Kun Xu, "Photonic measurement of microwave frequency based on phase modulation", *Optics Express*, Vol. 17 No. 9, Apr. 2009
- 10 H. Y. Xie, L. Wang, L. J. Zhao, H. L. Zhu and W. Wang, "Optical microwave generation using two parallel DFB lasers integrated with Y-branch waveguide coupler", *Chinese Physics*, Vol 16, No 5, May 2007
- 11 L. N. Langley, M. D. Elkin, C. Edge, M. J. Wale, U. Gliese, X. Huang and A. J. Seeds, "Packaged Semiconductor Laser Optical Phase-Locked Loop (OPPL) for Photonic Generation, Processing and Transmission of Microwave Signals", *IEEE transaction on microwave theory and techniques*, vol. 47, no. 7, Jul. 1999
- 12 A. J. Seeds, K. J Williams, "Microwave Photonics", *Journal of Lightwave Technology*, Vol 24, No 12, Dec 2006
- 13 X. F. Chen, Z. C. Deng and J. P. Yao, "Photonic Generation of Microwave Signal Using a Dual-Wavelength Single-Longitudinal-Mode Fiber Ring Laser", *IEEE Transactions on microwave theory and technologies*, Vol. 54, No. 2, Feb. 2006
- 14 X. F. Chen, J. P. Yao, and Z. C. Deng, "Ultra-narrow dual-transmission-band fiber Bragg grating filter and its application in a dual-wavelength single-longitudinal-mode fiber ring laser", *Optics Letter* Vol. 30, No 16, pp 2068-2070, Aug. 2005
- 15 Y. Yao, X. Chen, Y. Dai and S. Xie, "Dual-Wavelength Erbium-Doped Fiber Laser With a Simple Linear Cavity and Its Application in Microwave Generation", *IEEE Photonics Technology Letter*, Vol 18 No 1, Jan. 2006
- 16 Z. Yu, W. Margulis, O. Tarasenko, H. Knap and P.-Y. Fonjallaz, "Nanosecond switching of fiber Bragg gratings", *Optics Express*, Vol. 15, No. 22, Oct. 2007

- 17 M. Fokine, L. E. Nilsson, Å. Claesson, D. Berlemont, L. Kjellberg, L. Krummenacher and W. Margulis, "Integrated fiber Mach-Zehnder interferometer for electro-optic switching" *Opt. Lett.*, 27, 1643-1645. (2002)
- 18 http://optical-components.globalspec.com/learnmore/optics_optical_components/.../fiber_optics/optical_spectrum_analyzers, 15 May 2009
- 19 J. Kuhl and W. Schmidt, "Tunable Coherent Light Sources", *Applied Physics*, Vol 3, pp 251-270, 1974
- 20 Yu A. Varaksa, G. V. Sinitsyn and M. A. Khodasevich, "Modeling the gain and amplified spontaneous emission spectra of erbium-doped fiber amplifiers", *Journal of applied spectroscopy*, Vol. 73, No. 2, 2006
- 21 E. Desurvire, J. L. Zyskind and J. R. Simpson, "Spectral Gain Hole-Burning at 1.53 μm in Erbium-Doped Fiber Amplifiers", *Photonics Technology Letters*, Vol. 2, No. 4, Apr. 1990
- 22 I. Petterman, "Fibre Bragg Gratings: Realization, Characterization and Simulation", *Doctoral Thesis in Physics*, KTH, Sweden, 2007
- 23 Z. Yu, W. Margulis and P.-Y. Fonjallaz, "Manipulating light with Fibre Bragg Gratings", *VDM Verlag Dr. Müller Aktiengesellschaft & Co. KG*, Saarbrücken, Germany, 2008
- 24 R. Gafsi and M. A. El-Sherif, "Analysis of Induced-Birefringence Effects on Fiber Bragg Gratings", *Optical Fiber Technology*, Vol. 6, No. 3, pp 299-323. 2000
- 25 N. F. Borelli and R. A. Miller, "Determination of the Individual Strain-Optic Coefficients of Glass by an Ultrasonic Technique", *Applied Optics*, Vol.7, No. 5, pp 745-750, 1968
- 26 H. Knappe and W. Margulis, "All-fiber Polarization switch", *Optics Letters*, Vol. 32, No. 6, Mar. 2007
- 27 M. P. Fok et al., "Tunable dual-wavelength erbium-doped fiber laser stabilized by four-wave mixing in a 35-cm highly nonlinear bismuth-oxide fiber", Vol. 15, No. 10 / *Optics Express*, 5925, 14 May 2007
- 28 L. Xia, P. Shum, T. H. Cheng, "Photonic generation of microwave signals using a dual-transmission-band FBG filter with controllable wavelength spacing" *Applied Physics. B, Lasers and optics*, vol.:86 No:1, 2007